UiT The Arctic University of Norway

Faculty of Biosciences, Fisheries and Economics, Department of Arctic and Marine Biology

Linking methane fluxes and oxidation rates to methane oxidizing bacteria in an Arctic terrestrial methane seep, Svalbard

Franziska Nagel

Master's thesis in Molecular Environmental Biology – BIO-3950 – May 2020

Table of Contents

List of Tables

List of Figures

ANME	Anaerobic methane oxidation
BLAST	Basic local alignment search tool
CH_4	Methane
DAPI	4′,6-Diamidin-2-phenylindol
DNA	Deoxyribonucleic acid
dNTPs	Deoxyribonucleotide triphosphate
EBI	European Bioinformatics Institute
H_2O	Water
LP	Lagoon Pingo
MMO (sMMO / pMMO)	Methane monooxygenase (soluble/ particulate)
MOB	Methane oxidizing bacteria
PC	Polycarbonate
PCR	Polymerase chain reaction
PHB	Poly-β-hydroxybutyrate
qPCR	Quantitative polymerase chain reaction
RuMP	Ribulose monophosphate (pathway)

Abstract

Global warming has especially detrimental effects on Arctic regions. One major issue is permafrost thaw and sub-permafrost methane escape via surface seeps. While the mitigation potential of methane-consuming bacteria on marine pingo-like methane seeps is well described, terrestrial methane seeps are still understudied. Recently, open system pingos have gained attention as terrestrial methane seeps. Lagoon Pingo (N 78°14'22", E15°45'16"), a near-shore open system pingo in the Adventdalen valley, Svalbard, was chosen as a study site to investigate the potential impact of methane-oxidizing bacteria on methane evasion from open system pingos. During a fieldwork campaign in August 2019, methane fluxes were measured across the entire site and compared to the distribution of the site's methane oxidation potentials. The centre of evasion was found at the groundwater-discharging source. The discharged waters were carried away by an associated stream, which gradually emitted methane to a distance of up to 80 meters from the source. While waters from the site were not shown to possess the ability to oxidize methane aerobically, an abundance of methane oxidizing bacteria was found in sediments that were covered with methane emitting waters, creating the potential to oxidize methane. Furthermore, using Lagoon Pingo sediments as inoculum, enrichments have brought a methane oxidizing bacterial strain in culture. This novel *Methylobacter* sp. seems to produce exospores, a feature not previously described for cultured *Methylobacter* species. The new knowledge provided by this thesis is a fundament for evaluating the bacterial impact on methane evasion from open system pingos. This in turn could be used to improve predictions of the contribution of open system pingos to the global methane budget.

Keywords:

Methane oxidizing bacteria, Lagoon pingo, open system pingo, methane fluxes, oxidation rates, *Methylobacter*, Svalbard,

Acknowledgements

First of all, I would like to thank Alexander and Dimitri for their supervision! Thank you for all the explanations, help and advice! Your positive attitude is motivating and contributed greatly in making this thesis an enjoyable experience.

A special thanks to Pernille for all the lab work we did together, for the conversations about the topic, for all our conversations in general and most of all for becoming a good friend of mine!

In fact, everyone in the Methane research group had influence on this thesis by giving advice, giving small or large hints, or just by sharing their interests with me! Therefore, a very big 'thank you' to Anne Grethe and Mette for all the help with the enrichments, Tilman for the help with the 'gas stuff' and Alena for helping with the qPCR. I am grateful for the warm welcome I received from this research group and enjoyed being part of it.

Last but not least, deep gratitude to Colm, all my friends and family, who went through the last year with me. Not to forget, the 'Master's room group' – I enjoyed our time working, and not-working together.

1 Introduction

1.1 Methane in the environment

Arctic soils store large amounts of carbon, which may be released as carbon dioxide and methane as a result of global warming (Schuur et al., 2015). The Arctic warms more rapidly than other parts of the planet (Stocker et al., 2013), leading to increased methane emissions from thermokarst ponds and other landscape features produced by permafrost and glacier thaw (Wik et al., 2016). Methane has a stronger climate-warming potential than carbon dioxide (Isaksen et al., 2011) and its atmospheric concentration is increasing more rapidly than ever in recorded history (Ed Dlugokencky, NOAA/ESRL, link on p. 66). Wetlands are the largest natural methane sources, followed by geological seepage from reservoirs (Etiope and Milkov, 2004). Methane with geological origin is referred to as thermogenic methane, while methane with biological origin through methanogenesis is referred to as biogenic methane (Stolper et al., 2014). Methanogenesis is a microbial process primarily occurring in anoxic environments, such as deeper soil layers, wetlands, lakebeds, and permafrost thaw zones (Chan et al., 2005, Kotelnikova, 2002, McCalley et al., 2014). However, these methane-producing environments generally also accommodate microbial communities that mitigate the methane transit into the atmosphere (e.g. Deng et al., 2016, He et al., 2012, Tveit et al., 2013).

Besides carbon storage, the Arctic holds large reservoirs of methane as gas hydrates, structures of ice-scaffolds that trap gas molecules, predominantly in seabed sediments and terrestrial permafrost (Collett et al., 2011, Marín-Moreno et al., 2016). Cold climate environments are preserving the stability of these gas hydrates by two means. Firstly by isostatic depression, in which sub-glacial pressure and cold temperatures result in gas hydrate accumulation rather than gas evasion (Portnov et al., 2016). Secondly, continuous permafrost layers form a cap and confine gases to the sub-permafrost (Collett et al., 2011). When glaciers melt and sub-glacial pressure is lost, the underlying area is lifted (a process called isostatic uplift) and the gas hydrates destabilize, resulting in a gas discharge (Wallmann et al., 2018). Moreover, glacier retreat and permafrost thawing as a result of Arctic warming makes the cap more porous, enabling underlying free methane gases to escape their trap and seep into the atmosphere (Anthony et al., 2012). The resulting locations with high methane seepage, terrestrial or marine, are referred to as methane seeps.

1.2 Terrestrial methane seeps

Terrestrial methane seeps have been found across the planet, predominantly in the form of mud volcanoes, which were estimated to contribute between 20 to 40 teragrams per year to the global methane budget (Etiope et al., 2009a). The total number of onshore mud volcanoes is estimated to be higher than 926 (Dimitrov, 2002). Methane discharge through so-called macro-seeps, generally visible craters or vents, are categorised in three groups by Etiope et al. 2009: mud volcanoes, water seeps and dry seeps. According to this categorization, mud volcanoes discharge a mixture of gas, water and sediment. Water seeps discharge gases and water, which may be from groundwater, and dry seeps only emit gases (Etiope et al., 2009a). Furthermore, mud volcanoes are described to have three forms of gas seepage, macro-seepage, miniseepage and microseepage, depending on the gas flux intensity (Etiope et al., 2011, Spulber et al., 2010). Recently, another type of geological feature called pingos, which are common permafrost structures, have been recognized as potential terrestrial methane seeps. Some of Svalbard's pingos release large quantities of methane, highlighting the need to intensify research into this phenomenon (Hodson et al., 2020).

1.3 Methane consumption at methane seeps

In marine environments, numerous methane seeps occur as pockmarks, hydrothermal vents or mud volcanoes (Hovland et al., 2002, Milkov, 2000, Reeburgh, 2007). However, methane emitted from marine seeps does not reach the atmosphere unimpededly. It is consumed by microbes inhabiting the sediment and water column, thus reducing methane emissions to the atmosphere (Damm et al., 2005, Whiticar and Faber, 1986). The process of methane consumption by microbes is referred to as methane oxidation.

In contrast to the marine equivalent, the consumption of methane within terrestrial seeps is poorly understood and its potential estimated to be small. Etiope et al. deem the impact of methane oxidation on the emission from mud volcanoes to be insignificant (Etiope et al., 2009b). This study based on the meta-analysis of carbon isotopic compositions from more than 150 mud volcanoes, however, did not explicitly address microbial methane oxidation with microbiological methods. Nevertheless, the issue of microbial consumption in terrestrial methane seeps was lately subject to several studies, particularly targeting the microbial methane oxidation potential. These studies on mud volcanoes described methane producing and consuming microorganisms similar to those identified in marine methane seeps (Cheng et al., 2012, Niederberger et al., 2010, Wrede et al., 2012). In both the marine and terrestrial

environments, habitats were dominated by archaea involved in methanogenesis or anaerobic methane oxidation. However, based on low methanotrophic cell numbers, the microbial methane oxidation is assumed to be far less effective in terrestrial than in marine sites (Wrede et al., 2012). This assumption supports the Etiope et al. 2009 study. Whether or not methane oxidation is low in all terrestrial methane seeps is unknown. Therefore, in order to evaluate the methane budgets of terrestrial methane seeps, it is necessary to identify the size and location of methanotrophic communities and estimate their activity.

1.4 Methanotrophs

1.4.1 Physiology

Methanotrophs and methane oxidation metabolisms are divided into two distinctive groups according to the oxygen availability of the environment: aerobic methane oxidation performed by methane oxidizing bacteria (MOB), and anaerobic oxidation of methane by archaea (ANME). While MOB are found in oxygenic environments that contain methane, anaerobic oxidation by ANME has a major role in consuming sub-seabed methane, transforming the sediments into methane sinks (Bowles et al., 2019). MOB and ANME share the ability to use methane as a carbon and electron source, a process referred to as methanotrophy (Hanson and Hanson, 1996, Knittel and Boetius, 2009). However, this classical separation of bacterial and archaeal methanotrophs to either aerobic or anaerobic environments has been disrupted by the finding of bacteria, which perform aerobic methane oxidation under anoxic conditions (Ettwig et al., 2010, Raghoebarsing et al., 2006).

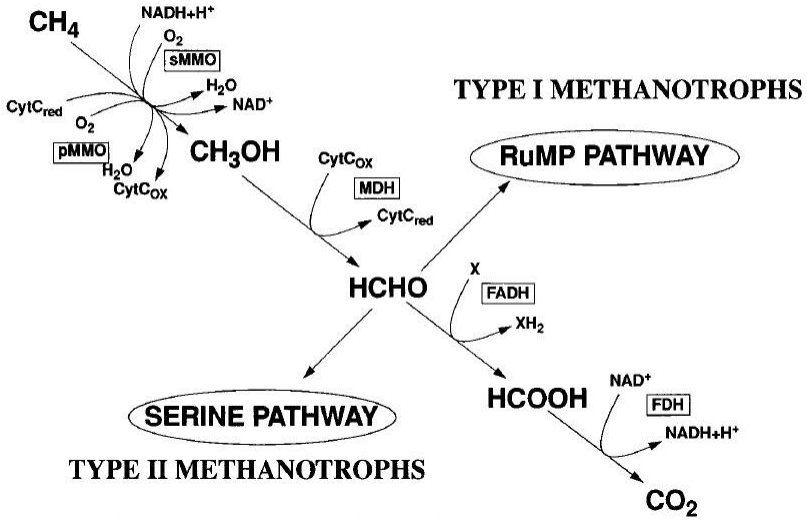

Figure 1: Methane oxidation pathways of MOB; figure from **Hanson and Hanson, 1996**. Abbreviations: CytC, cytochrome c; MDH, methanol dehydrogenase; FADH, formaldehyde dehydrogenase; FDH, formate dehydrogenase.

The fundamental enzymatic reaction of all known MOB is performed by the methane monooxygenase (MMO), appearing in a soluble (sMMO) and a particulate (pMMO) form (Semrau et al., 2010). Due to the ubiquitous presence of pMMO among methane oxidizing bacteria, the gene *pmoA*, encoding the β-subunit of the enzyme is generally used as a molecular marker for the detection of methanotrophs from aerobic environments (McDonald et al., 2008). Both pMMO and sMMO catalyze the oxidation of methane to methanol, using reducing agents and concomitantly converting molecular oxygen to water. In a further oxidation step, the methanol is converted by the enzyme methanol dehydrogenase to formaldehyde, which is either integrated into the organism's anabolic pathways to assimilate new cellular material or further oxidized to carbon dioxide. Two major carbon assimilation pathways exist in MOB, the ribulose monophosphate pathway (RuMP) and serine pathway. The chain of primary enzymatic reactions is depicted in **Figure 1**. Beside the RuMP and serine pathway, MOB were also found to utilize the Calvin-Benson-Bassham cycle for carbon assimilation (Khadem et al., 2011). Due to unspecific oxidation of hydrocarbons other than methane by MMOs (Burrows et al., 1984), MOB are also of interest for biotechnological applications and bioremediation (Jiang et al., 2010).

1.4.2 Phylogeny of methane oxidizing bacteria

Initially, MOB were grouped into two types based on phenotypical appearances: Type I and Type II. Among other phenotypical criteria, Type I MOB possess a bundled membrane-system in vesicles, often perpendicular to the cell boundaries, and use the RuMP pathway. Type II MOB on the other hand, possess a membrane-system arranged in parallel to the cell's periphery, and use the serine pathway (Davies and Whittenbury, 1970, Hanson and Hanson, 1996). This classification was validated by phylogenetic analyses for MOB within the phyla *Proteobacteria* and is therefore still commonly used. However, since the criteria used to describe Type I and II MOB are no longer exclusively found in these groups, this distinction may be inadequate to use without phylogenetic context (Knief, 2015, Op den Camp et al., 2009). Most described MOB cluster within the families *Methylocystaceae* (Type II) and *Beijerinckiaceae* of the class *Alphaproteobacteria,* and the family *Methylococcaceae* (Type I) of the class *Gammaproteobacteria* (Semrau et al., 2010). Exemplary genera of the family *Methylococcaceae* are *Methylobacter*, *Methylomonas*, *Methylomicrobium* and *Methylosarcina* (Bowman, 2016). The two genera of the family *Methylocystaceae* are *Methylosinus* and *Methylocystis* (Bowman, 2015). Outside the phylum *Proteobacteria*, MOB have also been found in the phylum *Verrucomicrobia* (Op den Camp et al., 2009).

1.4.3 Adaptations of methane oxidizing bacteria

Due to their existence in many different habitats, it is not surprising that a broad range of adaptations have been found among MOB, enabling them to cope with stressors and survive in extreme environments, such as deep-sea environments or high-temperature volcanic areas (Op den Camp et al., 2009, Skennerton et al., 2015). Knowing their adaptations to particular conditions might help to target the search for MOB on terrestrial methane seeps, which seems to be predominantly limited by oxygen availability in mud volcanoes (Alain et al., 2006, Wrede et al., 2012).

The presence of oxygen is crucial for the initial enzymatic reaction of aerobic methane oxidation. Nevertheless, active MOB have been found under oxygen-limiting conditions, revealing adaptations to bypass the need of a high oxygen availability. Within the *Gammaproteobacteria*, the ability to use oxidized nitrogen as alternative electron acceptors as well as having enzymes with different affinities have been suggested as adaptations to low oxygen concentrations (Kits et al., 2015, Skennerton et al., 2015). Metagenomic analyses brought insight into the genomic repertoire of several *Methylobacter* species to cope with oxygen stress and suggested it to be a highly competitive genus (Smith et al., 2018). Halo- and alkaliphilic MOB were found to grow at 1.5 M sodium chloride and pH 10.5, respectively. The ability to grow in highly alkalic environments seems to be coupled to the presence of salts and changes in the cell wall structure (Kalyuzhnaya et al., 2008, Khmelenina et al., 1999). Moreover, some MOB seem to possess cold adaptations. This became evident when true psychrophilic MOB, such as *Methylobacter psychrophilus* (Omel'Chenko et al., 1996) or *Methylospaera hansonii* (Bowman et al., 1997) were isolated, which show optimal growth at 5 – 10, and 10 – 13 °C, respectively. It was speculated that key adaptations for MOB to cope with low temperatures might be the formation of cysts or spores, or cell wall alterations (Trotsenko and Khmelenina, 2005). Based on metatranscriptomic data, activity of *Methylobacter* species in the environment during winter was shown, indicating a cold adaptation of members of this genus (Smith et al., 2018).

1.5 Pingo structures and Lagoon Pingo as a study site

Pingos are permafrost hills, elevated due to the expansion of an inner ice-core by the freezing of water (Gurney, 1998). More than 11000 pingos have been found across the Arctic, including Siberia, Arctic Canada, Greenland, Scandinavia (Samsonov et al., 2016). Approximately 80 were identified on Svalbard (Hjelle, 1993).

Pingos are classified in two major groups depending on the origin of the pressure that forces the ground water towards the surface: open- and closed system pingos. In open system pingos, groundwater inflow is supplied by hydraulic head, whereas the pressure from pore-water expulsion during freezing supplies the groundwater inflow in closed system pingos (Mackay, 1998). A groundwater discharge through springs can be associated with open system pingos (Yoshikawa, 1998). When the origin of pingos was first hypothesized, it was, among other theories, suggested that the rise of methane rich gasses would be responsible for pingo-growth [(Bennike, 1998) and references therein]. This suggestion was soon disproved, and the investigation of methane gasses evading from terrestrial pingos was not directly pursued until recently. However, it was suggested, already in 1995, that the inner-ice core of a pingo on Svalbard, named 'Lagoon Pingo', is accompanied by gases (Yoshikawa and Koichiro, 1995).

The evasion of gasses, primarily methane, has been repeatedly described for many pingo-like-features such as the so-called pockmarks at the seafloor, including the seas surrounding Svalbard (Paull et al., 2007, Portnov et al., 2016). Methane discharging pockmarks are not limited to offshore environments but also appear in fjords, such as the Adventdalen fjord (Forwick et al.). This is of interest in regard to Lagoon Pingo. Lagoon pingo, a nearshore pingo in the river-delta of the Adventdalen valley (**Figure 2**), is most likely derived from a former marine pockmark, which transitioned to a terrestrial pingo by isostatic uplift (Gilbert et al., 2018). It was estimated that only four pingos in Adventdalen are responsible for a 16 % increase in terrestrial methane emission of the valley (Hodson et al., 2020). Therefore, it was suggested to include pingos in greenhouse gas budgets (Hodson et al., 2019). Furthermore, this gives reason to the assumption that not only Lagoon pingo, but many more nearshore pingos worldwide are active terrestrial methane seeps and contribute to global methane emissions.

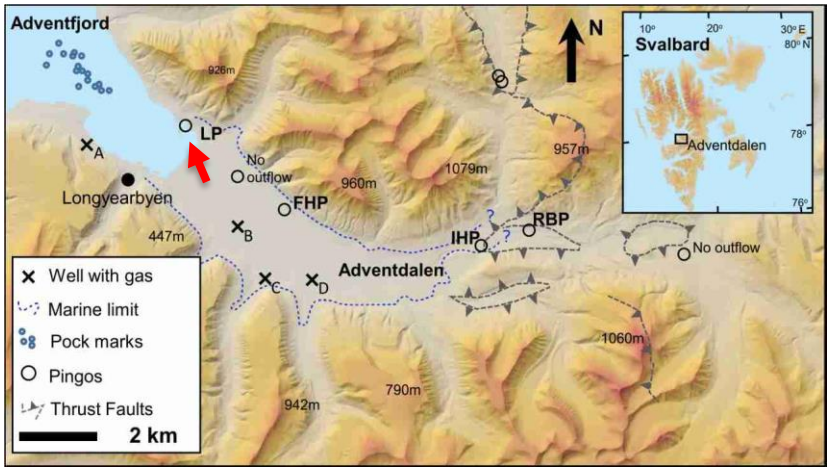

Figure 2: Schematic map of the valley of Adventdalen, depicting Pingos, pockmarks and wells. Lagoon pingo (LP) is highlighted with an arrow. Figure modified after **Hodson et al. 2020**.

Lagoon Pingo is described as an open system pingo, which is approximately four meters elevated from the surrounding grounds and covered by delta material (Yoshikawa and Koichiro, 1995). The number of sources and water discharging cracks reported varies between three (Hodson et al., 2019) and seven with regular new observations of crack formation with water discharge (Yoshikawa and Koichiro, 1995).

The water rising from the pingo core is anaerobic, contains a high concentration of gases, particularly methane, and salts. The pH tends to be neutral to alkalic (Hodson et al., 2019). The low δ_{13}C-isotopic signature of the methane discharged through the source and the absence of other hydrocarbons suggested that the methane is of biogenic origin, even though its source is not determined. Moreover, a variability in the methane δ_{13}C-isotopic signature also suggests partial oxidation (Hodson et al., 2020). The discharge of groundwater has resulted in the emergence of a pond structure, which may constitute a suitable habitat for microbial life, despite its seasonal variability from a pond to an icing-mound (**Figure 3**). In winter, the ice cover shields the water discharged from the pingo from atmospheric influences, resulting in a highly concentrated, anoxic environment under the ice-lid. In summer, an amalgamation of pingo-discharged water and meltwater create a pond structure exposed to atmospheric influences (Hodson et al., 2019). This seasonal variability may substantially affect microbial life on Lagoon pingo.

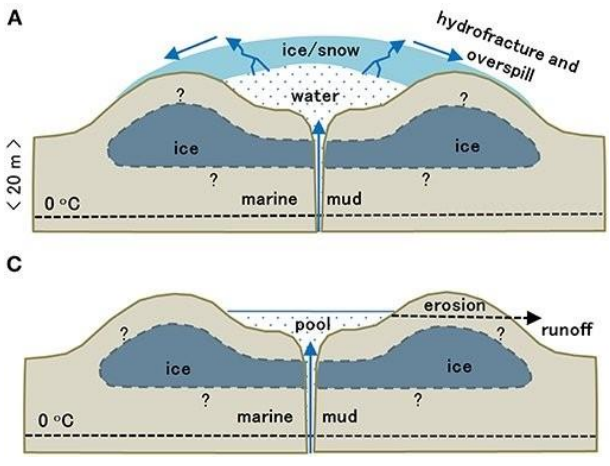

Figure 3*:* Cross-sectional depiction of LP in winter (**A**) and in summer (**C**), from **Hodson et al., 2019**, proposing its ice core and the suggested groundwater supply. Question marks indicate uncertainties.

Considering the presence of several necessities to support methanotrophy and the variable methane δ_{13}C-isotopic signature, Lagoon Pingo may accommodate an active methanotrophic community. Therefore, pingos may depict a so far undescribed habitat for methane oxidation, rather than a pathway of methane bypassing the gas hydrate seal. Since similar sites were found in Adventdalen (Yoshikawa, 1993) and pingos are common features in the Arctic, knowledge about methanotrophic activities in these sites is important to future estimates of sub-permafrost methane emissions.

1.6 Aim – Methane oxidizing bacteria on Lagoon Pingo

With this work I aimed to describe the methane fluxes of Lagoon Pingo (from now on abbreviated as LP) during the Arctic summer, whether MOB are present at this site and their distribution. Moreover, I aimed to explore the link between the methane flux pattern and the microbial methane oxidation potential. In order to achieve these aims, sampling efforts were made during a fieldwork campaign in August 2019 and analyses were performed as described in chapter 2.

Finally, my aim was to cultivate MOB from Lagoon pingo, obtaining one or several pure cultures of bacteria involved in methane oxidation at this site.

1.7 Hypotheses

Hodson et al. proposed that the groundwater discharge depicts the methane source of Lagoon Pingo (Hodson et al., 2019). However, Hodson et al. and Yoshikawa and Koichiro were inconsistent in their descriptions of the number of groundwater springs. Moreover, the study of Hodson et al. 2019 just provides an extrapolated estimate of methane evasion for the entire pingo, even though terrestrial methane seeps may be composed of macro-, mini-, and microseepages as described for mud volcanoes (Spulber et al., 2010). Consequently, a more complex methane evasion system than the sole emission from one spring was hypothesized:

1. *Methane emissions from Lagoon pingo are not limited to the discharge of the main source.*

It was shown on mud volcanoes, that a methanotrophic filter can exist on terrestrial methane seeps and that aerobic methane oxidation may occur in places where oxygen is not limiting (Alain et al., 2006, Wrede et al., 2012). However, the existence of MOB on open system pingos on Svalbard has not been shown before. Given the fact that LP provides all necessities for aerobic methane oxidation in summer and that MOB show many adaptations to cope with environmental stressors, it was hypothesized:

2. *Methane oxidizing bacteria are present on LP.*

After the initial methane oxidation results on site, which indicated that only the sediment oxidizes methane, it was assumed that the oxidation was caused by MOB. Therefore it was hypothesized that the spatial distribution of MOB is likely to be linked to the availability of methane, since methane is the primary energy source for all known MOB (Hanson and Hanson, 1996, Semrau et al., 2010).

3. *High methane availability, predicted by a high methane content in the sediments, results in an increased pmoA gene abundance.*

2 Material and methods

2.1 Site description

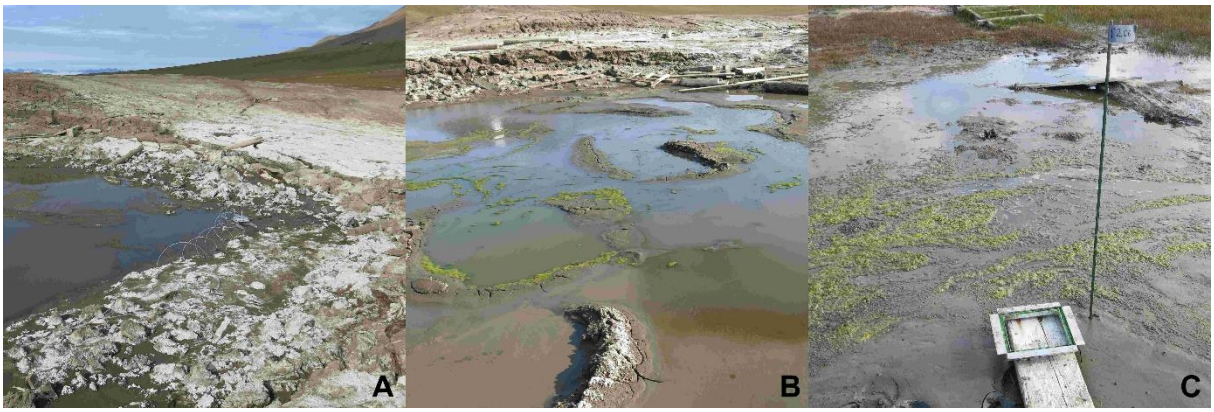

Figure 4: Photographs of LP-characteristics. **A**: the north-eastern borders of the pond and the dry pingo surface covered with salt crystals. **B**: the pond with the algae-biofilm, view towards south east. **C**: the transition from the stream to biofilm-dominated wetlands and the grass-vegetated grasslands in the background; view towards east.

Lagoon Pingo is located in the proximity of Longyearbyen, Svalbard, and by the delta of the Adventdalen river (N 78°14'22", E15°45'16", **Figure 2**). The centre of the pingo forms a crater-like pond surrounded by dry sediments that were fully covered with salt crystals, as previously observed [**Figure 4**, **A**; (Hodson et al., 2019, Yoshikawa and Nakamura, 1996)]. No vascular plants grow on LP. Vascular plants can depict another mean of transferring subsurface methane to the atmosphere (Schütz et al., 1991). Therefore, the absence of vascular plants simplifies the system by limiting methane emissions to direct surface-atmosphere interfaces. However, an algae-biofilm was visible on the water surface, noticeably growing during the fieldwork campaign (**Figure 4**, **B**). Extensive algae-biofilms and patches of moss were observed at approximately 80 m distance from the source, followed by typical tundra vegetation with sedges and grasses (**Figure 4**, **C**). The air temperature in 2019 before the fieldwork varied between -30.3°C and +14.9°C, with an average temperature of +8.4°C in July, the warmest month of the year 2019 (**Figure 5**, for reference see figure text).

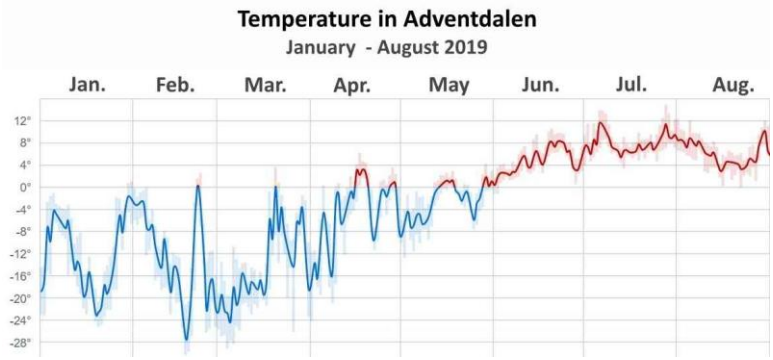

Figure 5: Adventdalen temperature profile from January to August 2019. Graph taken from https://www.yr.no. For full link see p. 66.

2.2 Fieldwork

To describe the site and investigate whether a microbial filter for methane exists, samples and information about environmental parameters were gathered during a fieldwork campaign in August 2019.

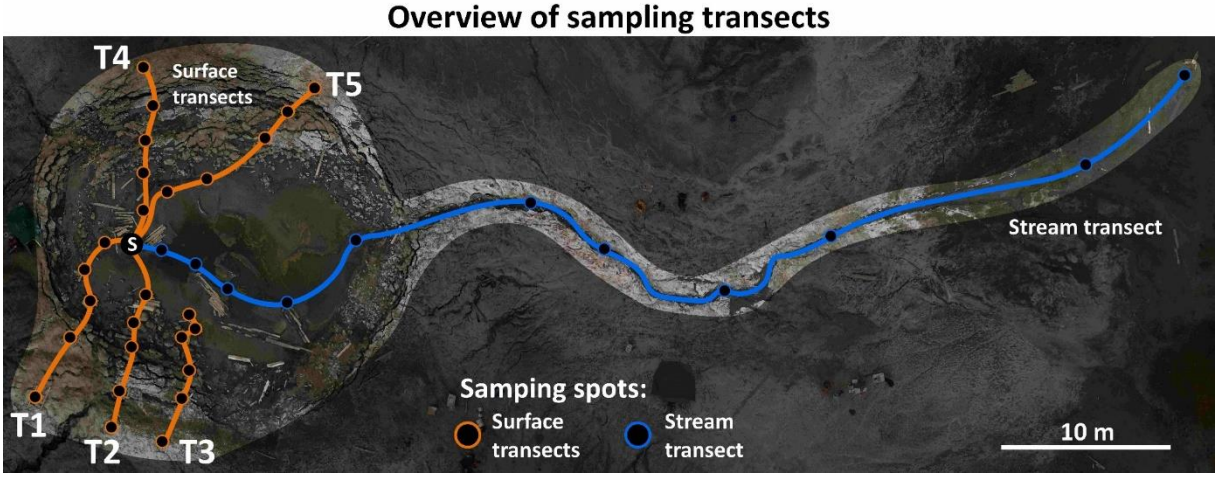

Figure 6: Overview of the transects; in orange: The 5 radial 'Surface' transects starting from the source outwards; with transect indices. In blue: Transect 'Stream' following the water flow. All sampling spots depicted by black dots (see explanation within the figure). The source, from which all transects (except for T3) start, is indicated with an S.

Six transects radially stretching outwards from the groundwater source were assigned (**Figure 6**). Five transects (named T1 to T5) started at, or close to the source and stretched up to 16 meters across the different surface types surrounding the pond (**Figure 6**, orange lines). These five transects are referred to as surface transects. Each of these surface transects comprised six sampling spots, named C1 to C6. For example, the fourth sampling spot of the second transect would be T2C4. At each sampling spot, delineated by the chamber frame used for methane flux measurements (see 2.2.1), samples for DNA analysis, chemical description (pH, methane and water content) and methane oxidation experiments were collected, and the methane flux was measured. The sixth transect with 12 sampling spots followed the water flow from the source, along the stream until the point at which the water reached flat, vegetated grounds (**Figure 6**, blue line). For this stream transect (abbreviated as TS), sampling was performed as described for the five radial surface transects. Additionally, oxygen concentrations in the stream water were measured.

2.2.1 Methane flux measurements

Net methane fluxes were measured in a closed system with a continuous measurement, using specially tailored acrylic glass chambers with a volume of 3603 cm^3. The chambers were covered with aluminium foil to decrease sun-induced heating within the chambers during the measurement. Each chamber was placed onto an aluminium frame using a putty seal to create

a gas-tight chamber. The chambers were connected to a recirculating multiplexer (eosMX-P, Eosense; Dartmouth, Canada) transmitting the gases to a laser spectrometer greenhouse gas analyser (U-GGA-915, Los Gatos Research, San José, USA) using inert, gas-tight perfluoroalkoxy tubing (inner diameter ~ 4 mm, length 7.5 or 10 m, respectively). Chambers, tubing, and the analyser were flushed with air prior to each measurement. The methane flux measurements had a duration of 5 minutes, except for water-surface measurements, where due to high methane emissions measurements were shortened to one minute at the source and to three minutes along the stream transect. Due to the short length of individual flux measurements, the effect of chamber temperature on the estimated flux was negligible. The net methane fluxes were determined based on the linear regression calculated by the eosAnalyze software (Version 3.7.9 - custom made; Eosense, Dartmouth, Canada). All methane flux measurements were performed in cooperation with Tilman Schmider.

2.2.2 Oxidation rate estimations

Closed-batch incubations of sediments and water were used to determine methane oxidation rates. Approximately 14 ($\pm$ 7.5) g of sediment or 12 ($\pm$ 3.7) mL of water were transferred from the respective sampling spot into 120 mL serum bottles, which were thereafter sealed with sterile butyl-rubber stoppers (10 x boiled) and crimp-caps. To enrich the headspace of the serum bottles, methane was injected into each bottle with a gastight syringe. The amount of methane injected corresponded to the expected environmental methane levels: 10 mL of 1000 ppm methane for sediment samples from the surface transects and 0.1 mL pure methane for samples (water and sediment) from the stream transect and source sediments. Flux measurements had indicated the stream to be the carrier of methane while less methane was diffusing through surface sediments outside the stream. The rationale was that in order to reliably detect low methane oxidation rates by small communities, a low concentration is necessary to give a smaller measurement error. However, this approach makes direct comparisons of potential rates between the stream and surface transects problematic. The methane concentrations were measured in the headspace of all bottles immediately after injection (t_0) and at least once every 24-hours for the next three days. All flasks were incubated for the first 8 hours on site (6 to 17°C) and the remaining time in the field laboratory incubator at 10°C. All incubations were performed in duplicates. Methane concentration measurements were performed with the LGR greenhouse gas analyser using ambient air as a carrier (Gonzalez-Valencia et al., 2014).

To estimate the oxidation rates (equation **3**), the measurements of incubation day two and day three were chosen. The headspace volume was estimated using a conversion factor, determined on test bottles (see equation **4**, p. 69), that calculates the sample volume according to its previously assigned category (see 2.4.1) and weight. Using the ideal-gas-law and the averaged incubation temperature and headspace-pressure, the amount of methane within the headspace was calculated for the two days (see equation **1** & equation **2**). The differences in the amount of methane in the headspace were then divided by the time in between the measurements and the wet weight of the incubated sediment to obtain the oxidation rate (see equation **3**).

$$Ideal\ Gas\ Law: P * V = n * R * T \qquad \mathbf{1}$$

In which *P* is the pressure, given in bar [bar]; *V* is the volume, given in litre [L]; *n* is the amount of substance of the respective gas, given in moles [mol]; *R* is the ideal gas constant [$\sim 8.314 * 10^{-2}\ \frac{L * bar}{K * mol}$]; and *T* is the temperature, given in Kelvin [K].

$$Amount\ of\ substance\ n_i = \frac{P_m\ [bar] *\ V_i\ [L]}{R\ \left[\frac{L\ *\ bar}{K * mol}\right] *\ T_m[K]} \qquad \mathbf{2}$$

In which *m* indicates the mean of the parameter and *i* indicates the respective incubation.

$$Oxidation\ rate\ [nmol * g\ soil^{-1} * h^{-1}] = \frac{n_{i=2}[nmol] - n_{i=3}[nmol]}{m_{ww}\ [g] * t[h]} \qquad \mathbf{3}$$

In which *m* is the mass of the sample incubated in wet weight (index *ww*), given in gram [g]; and t is the incubation time in hours [h].

However, this calculation was based on the timeframe with the highest rate. Therefore, all datasets were manually assessed in comparison to the negative control to identify false positives and false negatives prior to calculation. All calculations performed with Microsoft® Excel® (Office 365, Version 16.0; Microsoft, Redmont, USA). All measurements for the estimation of methane oxidation rates were performed in cooperation with Tilman Schmider.

2.2.3 Determination of physical and chemical sediment properties

The sediment pH was determined with a 1:5 (w/w) dilution of the sediments with deionized water. The water content was determined by drying the sediments from the serum bottle from the oxidation rate estimations at 105°C for 20 hours. Oxygen concentrations of the stream water were determined using a Clarks type electrode (OX-100, Unisense, Aarhus, Denmark). The

methane content of the sediments was determined as follows and is based on the method by Magen et al. (Magen et al., 2014): 1 mL of sediment was inserted in an exetainer and 1 mL headspace was exchanged with 1 M NaOH for preservation. The exetainers were stored at 6°C until further use. In the laboratory, 0.5 mL of fully saturated NaCl solution was added to the exetainers, whereby 0.5 mL of the headspace was simultaneously retrieved into a gas-tight syringe and injected to a gas chromatograph (GC; Modell: SRI 8610C, SRI Instruments, Torrance, USA) equipped with a Flame-Ionization Detector and using hydrogen gas as the carrier gas. The oven temperature was set to 40°C. The injection size was 0.5 mL. A reference curve was produced using commercial standard gases. The methane content of all sampling sites was estimated in duplicates. The measurements named above were performed in a collaboration of all group members. Calculations of the methane content of the sediments were performed by Dimitri Kalenitchenko and Tilman Schmider.

2.3 Laboratory

2.3.1 Total nucleic acid extraction

Total nucleic acids were extracted using a phenol-chloroform extraction protocol as described by Angel et al. 2012 (Angel et al., 2012). Nucleic acids were extracted in cooperation with Pernille Fåne.

From each sampling location, sediment was transferred into sterile plastic tubes and frozen immediately in liquid N_2. In the laboratory, the frozen sediments were crushed in sterile plastic bags. Resulting pieces were mixed, and a subset of randomly chosen pieces were ground using sterilized grinding jars made from stainless steel and a tissue lyser (TissueLyzer2, Qiagen, Hilden, Germany), in order to achieve a randomized homogenization of the sample. Ground samples of approximately 0.2 ($\pm$ 0.02) g wet weight were transferred into precooled Ribolyser tubes (Lysing Matrix E; MP Biomedicals, Santa Ana, USA) and stored at – 80°C until further processing. Nucleic acids were extracted in duplicates using a TNS extraction buffer (see p. 67). The samples were cooled with liquid N_2 throughout the entire process. The air-dried nucleic acids were resuspended in 50 µL nuclease-free water with 0.5 µL RiboLock RNase inhibitor (Thermo Fisher Scientific, Waltham, USA). Nucleic acids were stored at -80°C until further use. The DNA content of the extracted nucleic acids was measured with the Qubit® 2.0 fluorometer and the Qubit® DNA dsDNA HS Assay Kit (Thermo Fisher Scientific) according to the manufacturer's instructions. Qubit® measurements were performed by Pernille Fåne.

2.3.2 Quantitative PCR (qPCR)

The *pmoA* and 16S rRNA gene were amplified using a quantitative PCR approach. To minimize amplification bias and simultaneously decrease PCR inhibition, all samples were adjusted for the same DNA amount (0.1 ng) per reaction. The total reaction volume was set to 15 µL containing SsoFast™ Evagreen® Supermix (Bio-Rad, Hercules, USA), the respective amount of DNA and 0.2 µM of forward and reverse primer. An overview of the amplification temperatures is given in **Table 1**. The standard curve was constructed using triplicates of 10^6 to 1^0 gene copies of *Methylobacter tundripaludum* DNA. The genome of *Methylobacter tundripaludum* is available and reveals one copy of the *pmoA* gene and two copies of the 16S rRNA gene, which was considered during data analysis. For *pmoA* amplification the primer set 189 forward and 601 reverse were chosen (Kolb et al., 2003); for 16S rRNA gene amplification the set BAC1369F (Suzuki et al., 2000) and BAC1492R (Weisburg et al., 1991). The primer set 189f and 601r was established by Kolb et al. 2003 to target MOBs of the *Methylobacter* and *Methylosarcina* groups, and therefore represents a limitation to the method. However, this limitation was knowingly accepted, because of the general dominance of *Methylobacter* in the environment and the fact that *Methylobacter* has been found associated to an Arctic methane seep and Svalbard soils (e.g. Belova et al., 2014, Smith et al., 2018, Wartiainen et al., 2006). Moreover, preliminary data analysis of the sequencing results of the master's thesis of Pernille Fåne verified *Methylobacter* to be the dominant genus on LP.

The results are firstly presented as copy numbers per g wet weight, and thereafter presented as a ratio of *pmoA* to 16S rRNA gene copy numbers. The copy numbers of the16S rRNA gene are referred to in a shortened name as 16S copy numbers or 16S abundance. For the calculation of the gene ratio, results were removed when amplifications of both genes showed more than one melt peak, or a melt peak with a melt temperature deviating from the standard. If only the amplification of *pmoA* showed erroneous melt peaks, but not the amplification of the 16S rRNA gene, the ratio was set to 0. For further information see appendix, p. 64. Relative copy numbers instead of cell numbers were used to avoid misinterpretations due to false assumptions about exact copy numbers per cell, since they can vary greatly (Dunfield et al., 2007, Semrau et al., 1995, Vetrovsky and Baldrian, 2013). Therefore, a greater dominance of MOB was inferred from comparably higher copy number ratios.

Table 1: Amplification cycles used in qPCR; Reactions were kept similar for the amplification of the *pmoA* and 16S rRNA gene apart from primer-related annealing temperature deviations.

PCR step	*pmoA*		16S	
Initial denaturation	95°C	02:00	95°C	02:00
Cycle denaturation	94°C	00:25	94°C	00:25
Annealing	**54°C**	00:20	**56°C**	00:20
Elongation	72°C	00:45	72°C	00:45
Plate read	82°C	00:10	82°C	00:10
Final denaturation	93.5°C	00:05	93.5°C	00:05
Melt Curve	from 60°C to 95°C (0.5°C increment		from 60°C to 95°C (0.5°C increment	

2.3.3 MOB Enrichment & Isolation

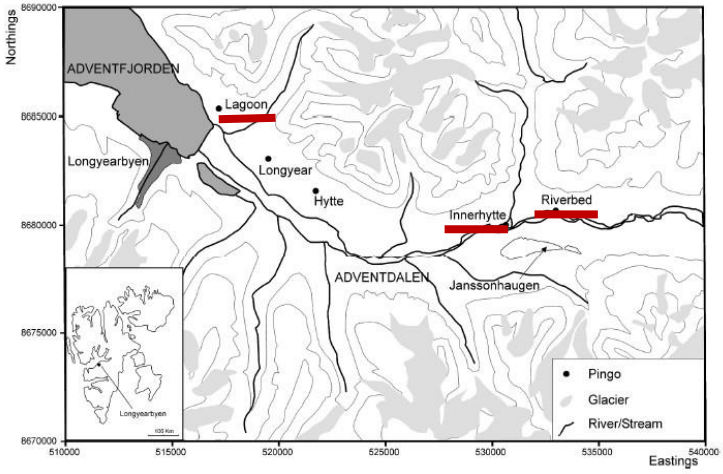

Figure 7: Sample origins for enrichment of MOB from Adventdalen pingo sites. **Modified after Ross et al. (2007).**

Two types of environmental samples were used to enrich for methanotrophic bacteria: (a) Water and snow samples from Adventdalen pingos (Lagoon, Innerhytte, Riverbed; see **Figure 7**) on Svalbard, Norway and (b) sediment samples from the Lagoon Pingo taken during fieldwork in August 2019.

Water and melted snow samples were filtered in an appropriate dilution through Whatman polycarbonate (PC) filters (0.2 µm pore size; Whatman - GE Healthcare Life Sciences, Chicago, USA). Appropriate dilutions were estimated based on vacuum-filtered trials with SYBR green (Thermo Fisher Scientific) stained cells. The filters were placed on the surface of 10 x diluted NMS media (Dunfield et al., 2003, Whittenbury et al., 1970b) pH 7.2, in petri dishes (Svenning et al., 2003). The filters were incubated at 20 % methane in ambient air (v/v) at 10°C. After

establishing colony growth, a randomly chosen representative colony was used for further enrichment. All work was performed at 6°C to reduce stress as the temperatures at the sites of origin rarely exceed 10°C (**Figure 5**, further reference can be found on p. 64).

Sediment samples with a high observed oxidation rate were used to enrich for MOB from LP. The serum bottles, stored at 4°C since the fieldwork, were injected with 15 % methane in the headspace and 10 x diluted NMS in a 1:1 weight to volume ratio (1 g : 1 mL). The media was adjusted to two pH-values; pH 8.7 to mimic the sample's origin, and pH 7.2 to simulate a neutral environment. After 3 weeks, methane oxidation was verified using gas chromatography (as explained in 2.2.3) and slurry was sampled aseptically. A dilution of the slurry in NMS-media was filtered onto PC filters (Whatman) as described for the water samples. The filters were placed floating on 10x diluted NMS media of the respective pH levels and incubated at 10°C in darkness. A reference for the media compositon of NMS can be found on p. 68.

For all enrichments, isolation was pursued by repeatedly picking, diluting and re-streaking colonies onto filters and agar plates, respectively. Isolation in liquid media in serum bottles containing 20 % methane in the headspace was attempted but without success as was the cultivation on agar plates.

2.3.3.1 Phylogenetic characterization

Respective colonies of each sample were lysed in 20 mM NaOH at 99°C for 6 minutes. Thereafter, the mixture was spun in a table-centrifuge for approximately 30 seconds. The DNA containing supernatant was used for PCR amplification of the *pmoA* gene with the primer set 189F/661R (Costello and Lidstrom, 1999). The total reaction volume was 25 µL and composed as follows: For each reaction, 11.65 µL H_2O, 2.5 µL 10x buffer, 5 µL Q-solution, 0.75 µL $MgCl_2$ (50 mM), 0.5 µL dNTPs (10mM), 1.25 µL primers (10 µM), 0.1 µL Taq-polymerase, 2 µL template (Qiagen, Thermo Fisher Scientific & VWR, Radnor, USA). The gene product was separated by gel electrophoresis and purified by cutting the respective band and centrifuging it through a glass fibre filter (Whatman). The PCR products were sequenced with Sanger technique using the BigDye® Terminator kit (Thermo Fisher Scientific). Labelling reactions for sequencing were composed as follows: 2.5 µL H_2O, 1.0 µL sequencing buffer, 2 µL 2.5x BigDye®, 2 µL forward primer (0.8 µM), 2.5 µL template. PCR and nucleotide labelling settings are described in **Table 2**.

Table 2: Amplification cycles of PCR and labelling of *pmoA* sequences.

PCR step	*pmoA* (189f & 661r)		Big Dye (189f)	
Initial denaturation	94°C	05:00	96°C	01:00
Cycle denaturation	94°C	01:00	96°C	00:10
Annealing	58°C	01:00	56°C	00:05
Elongation	72°C	01:00	60°C	04:00
Final Elongation	72°C	10:00	-	-
Cool-down	4.0°C	10:00	4°C	01:00

2.3.3.2 Phylogenetic analysis of the sequences

The *pmoA* sequences obtained by Sanger sequencing were analysed for their relationships using Mega-X [Version 10.1.1, (Kumar S. et al., 2018)]. Additionally, all sequences were BLAST aligned to the online NCBI nucleotide database. Multiple sequence alignment was achieved using ClustalW (Thompson et al., 1994). For phylogenetic tree construction, the sequences providing the first BLAST search alignments and reference sequences representing related isolates, retrieved from the European Nucleotide Archive (links on p. 66 - 67), were used. Tree construction was based on the Minimum Evolution method (Rzhetsky and Nei, 1993), obtaining bootstrap values from 500 replicates. Pairwise distances were calculated by the p-distance model.

2.3.3.3 Morphological characterization

Fluorescence in situ hybridization was applied to distinguish the morphology of MOB from contaminants. Cells were harvested and fixed overnight at 4°C using paraformaldehyde (4 % w/v). Fixed cells were pelleted and resuspended in 1 x PBS and 0.1 % Tergitol NP_{40} (Sigma-Aldrich, St. Louis, USA) to wash from media. Thereafter, the cells were again pelleted and resuspended in 20 to 200 µL storage solution and an equal amount of 96% pure ethanol. Cell suspensions were stored at -20°C until further use.

Cells were spotted onto poly-L-lysin coated 10-well microscopy slides (Merck, Darmstadt, Germany) followed by a dehydration series in ethanol dilutions (50%, 80%, 96%). The air-

dried cells in each well were then hybridized with 50 ng probe in hybridization solution in dark and air-tight chambers at 37°C for 2.5 hours.

Post-hybridization washes were performed as follows: firstly, the slides were rinsed with pre-warmed (37°C) washing solution 1, followed by an incubation in pre-warmed washing-solution 1 at 37°C. Thereafter, cells were counterstained with 4′,6-Diamidin-2-phenylindol (DAPI) at RT, before the slides were washed at 37°C in washing solution 2. Before mounting, the cells were washed in MQ-water and air dried. For the detection of MOB cells, the Type-I-MOB specific probe MG-64 (Bourne et al., 2000) was used, while hybridization effectiveness was evaluated using the 16S rRNA probe EUB338 (Amann et al., 1990). For either type of probe the SV96 strain of *Methylobacter tundripaludum* (Type I MOB) was used as a positive control. As negatives, the SV97 strain of *Methylocystis rosea* (Type II MOB) and the archaeal *Methanobacterium formicum* were used for the MG-64 and EU338 probe, respectively. Buffer and reagent composition can be found in the appendix, p. 68.

The hybridization was evaluated using a fluorescence microscope (Axio Observer Z1; Zeiss, Oberkochen, Germany). To detect DAPI stained cells, a UV-filter set (Excitation: BP 365, Emission: LP 420; Filter Set 02, Zeiss) was used, while for the detection of the Cy3-labelled probes a red-filter (Excitation: BP 545/25, Emission: BP 605/70; Filter Set 43, Zeiss) was used. Light Microscopy images to determine the homology of cell morphologies were taken using the Axiovert 200M Microscope (Zeiss). All image processing performed with ImageJ 2.0.0-rc-69 (Schindelin et al., 2012). Brightness and contrast were increased in all pictures.

2.4 Statistical analysis

For all statistical analyses, a confidence interval of 95% was chosen, so results were accepted as significant when $p < 0.05$. Water samples from the oxidation rate experiment were excluded prior to statistical analysis. For univariate analyses, sampling spots with missing values were removed. For multivariate analyses, missing values were treated as follows: all measurements of T1C1 and T2C2 were removed, due to sparse data collection. The missing water content value for T5C1 was replaced by the average of water contents of all source sediments. For missing *pmoA* to 16S ratios, a category average (see 2.4.1) was used.

2.4.1 Categorization of the sediment samples

The sediment samples were assigned one of the categories described in the following **Table 3**, according to the origin of the sediment sample and its physical appearance. The distribution of the categories on LP is depicted in **Figure 8**.

Table 3: Categorizing of the samples according to their origin and appearance.

Category	**Reasoning**
Source	Sediment directly bordering the source and being in contact with source water
Still pond	Sediments from water-covered locations that did not exhibit any water-movements
Wet mud	Clay-like sediments, not covered by water from the pond but appeared water soaked
Dry soil	Soil with no obvious contact to water, generally covered with salt crystals and from elevated areas in comparison to the pingo pond
Miniature source (Mini source)	Sediments taken from locations with subsurface-water discharge; much smaller than the main source of the pond
Pond flow sediment	Sediment from locations covered with water flowing towards the stream, but still part of the pond
Stream flow sediment	Sediments from beneath the stream

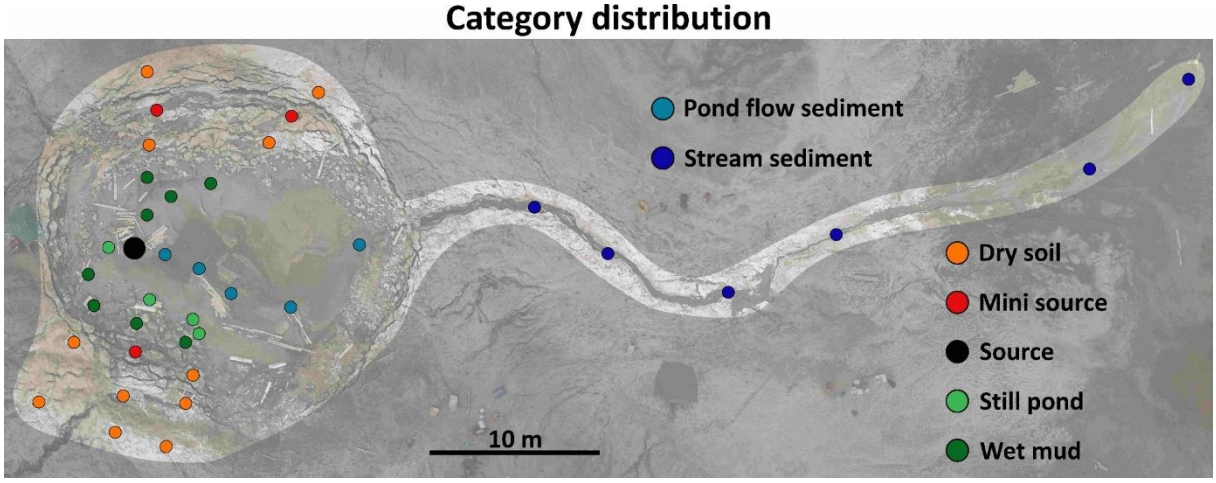

Figure 8: The distribution of the categories allocated to the sediment samples.

Prior to analysing the data in accordance to sediment categories, the sediment samples were screened to identify whether the categories were represented by the measured predictor variables and to test whether the categories differ significantly. The clustering was performed using the least-squares method 'Ward's hierarchical clustering' to create clusters with minimal variance as described in Borcard et al. 2011 (Borcard et al., 2011). The predictor variables, distance to the source, pH, methane flux, water and methane content were normalized during the procedure. The tree was cut at a tree height of 1 after visual examination and three of the clusters were extracted. Due to non-normal distributions tested with the shapiro.test() function of R, a nonparametric comparison test for multivariate samples to test for significant differences was performed using the 'npmv' package of the CRAN R project (Burchett et al., 2017). The test was based on 1000 permutations and the ANOVA-like statistic. A pairwise comparison was performed with the ssnonpartest() function of the same package with a confidence interval of 95 %. A table of relative effects was obtained as an output of the latter function. The results can be found in the appendix p. 63.

2.4.2 Statistical testing

Prior to analysis, normality and homogeneity of the variances were tested using the shapiro.test() and bartlett.test() function, respectively. A Kruskal-Wallis was performed to test the differences in *pmoA* abundances between the categories using the kruskal.test() function of R. A two-way ANOVA test was performed to test the differences between the *pmoA* to 16S ratios of firstly the pingo surface and the stream, and secondly the sediment categories. Student's t-tests were performed using t.test(), after assessing normality as described above and equal variances using var.test().

2.4.3 PCA and linear regressions

For PCA, missing values were replaced as described above. All variables were log transformed to increase normality and linearity. Outliers were not removed to obtain an ordination of all sampling spots. The PCA was performed using the prcomp() function of R and as described in Borcard et a. 2018 (Borcard et al., 2018).

Linear regression models were calculated with the lm() function of R. Normality was tested as described above. Homoscedasticity was tested with the Breusch-Pagan test and the ncvTest() function of the 'car' package (Fox and Weisberg, 2019). To optimize the models, the surface and stream transects were separated. To test for significant slopes of the linear regressions, an ANOVA test was performed on the linear regression using anova() function of R.

A linear regression was generally accepted when the R^2 value was larger than 0.55, homoscedasticity was not violated, and a regression ANOVA test verified the slope to be significant. Regressions were also rejected when they were skewed by few observations. Further information about the regression models can be found in **Table 9** (appendix p. 65).

3 Results

3.1 Methane oxidizing bacteria on Lagoon Pingo

3.1.1 Methane fluxes

Methane fluxes were measured using closed chambers ($n_{sampling\ spot} = 2$). From the water surface of the stream transect, average methane fluxes range from - 0.5 to 1650 nmol/m^2/s, with most measurements detecting fluxes in the magnitude of several hundred nmol/m^2/s (blue line in **Figure 9**). A decrease of methane fluxes with increasing distance to the source was observed in the stream transect. The average methane flux of the source was 1335.3 (± 260) nmol/m^2/s ($n_{source} = 9$). Among the surface transects (orange lines in **Figure 9**), the three sampling spots T2C4, T4C5 and T5C5 exhibited between one and two orders of magnitude higher methane fluxes than the surrounding sampling spots and were therefore called miniature sources. The corresponding sediment category has the name 'Mini source'. T2C4 emitted on average 687.4 nmol/m^2/s, T4C5 emitted on average 375.0 nmol/m^2/s, and T5C5 emitted on average 42.0 nmol/m^2/s. In comparison, the average methane flux of the surface transects (excluding the source and miniature sources) was 0.7 nmol/m^2/s. The appearance of the so-called miniature sources varied (see **Figure 28**, p. 64). T2C4 was a waterlogged area in which methane ebullition was observed. T4C5 had a volcano shape with water seeping from the centre. T5C5 was a small volcano-like opening in the sediments. Three sampling spots exhibited negative average methane fluxes: T4C4, T5C2 and TSC12, with averages of – 0.1, 0.2 and – 0.6 nmol/m^2/s, respectively.

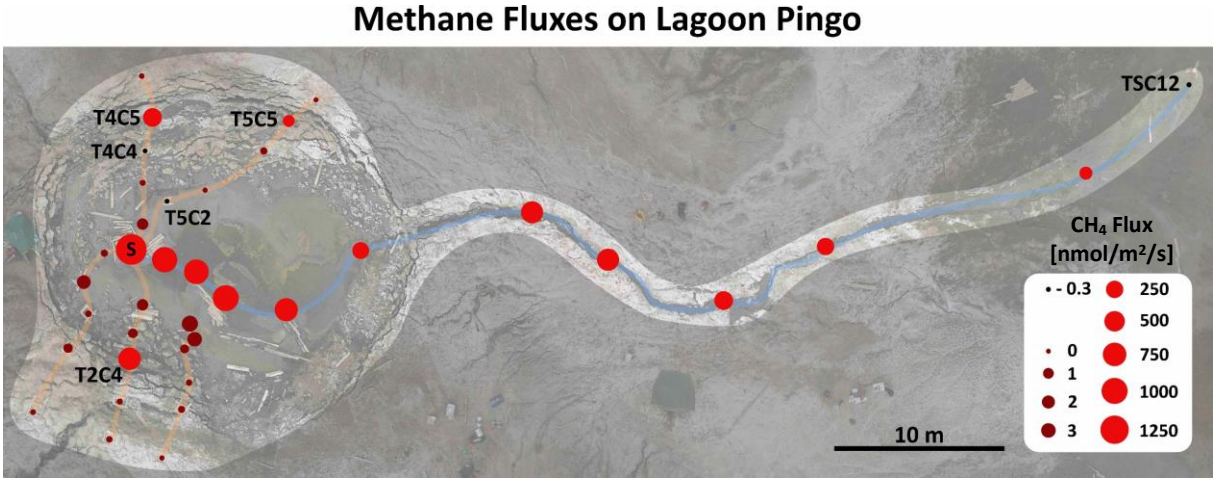

Figure 9: Methane fluxes on Lagoon Pingo; Average methane fluxes in nmol/m^2/s are depicted as the sizes of red and black circles (see legend for sizes). The main source is annotated with an S. For the measurements of T4C4, T5C2 and TSC12, the average is given.

3.1.2 Methane oxidation

To investigate the methane oxidation potential of MOB on LP, sediment and water samples were incubated in serum bottles under a methane enriched atmosphere. The methane concentration change between day two and three was used to estimate the oxidation rate.

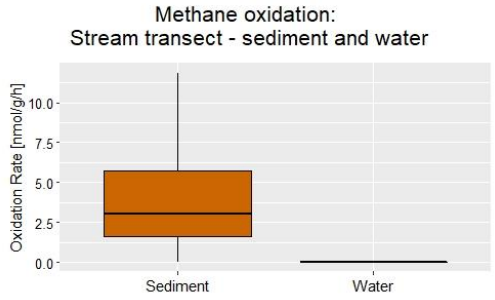

Figure 10: Oxidation rate comparison between sediment and water samples from the stream transect.

No water sample from the stream transect was found to oxidize methane under the given conditions (**Figure 10**). On the other hand, the sediment samples from the stream transect oxidized with an average rate of 3.99 nmol/g/h. Therefore, further analyses focused on the sediment samples.

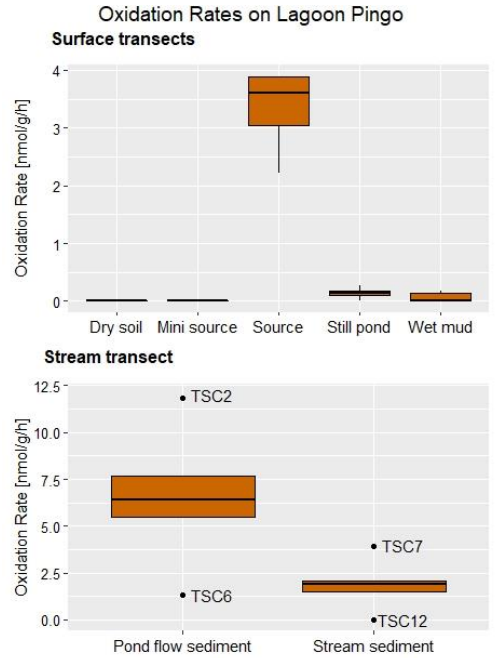

Figure 11: Oxidation rates on LP according to their category and divided into 'Surface transects' and 'Stream transect'.

Among the sediment categories from the surface transects, the 'Source' sediment exhibited the highest oxidation rate with an average of 3.15 (± 0.8) nmol/g/h (**Figure 11**). The categories 'Still pond' and 'Wet mud' had much lower oxidation rates in comparison [0.14 (± 0.11) and 0.055 (± 0.08), respectively]. The categories 'Dry soil' and 'Mini source' did not exhibit methane oxidation. The stream category 'Pond flow sediment' had the highest oxidation rate of all categories with an average of 6.55 (± 3.8) nmol/g/h, whereas the 'Stream sediment' samples had an average oxidation rate of 1.87 (± 1.3) nmol/g/h. TSC12, the sampling spot with the greatest distance to the source, was the only stream transect sample which did not oxidize methane.

3.1.3 Nucleic acid analyses

3.1.3.1 DNA content

DNA was extracted from all samples to be used as template for qPCR. However, the amount of DNA in the samples is itself a rough indication of the amount of biomass.

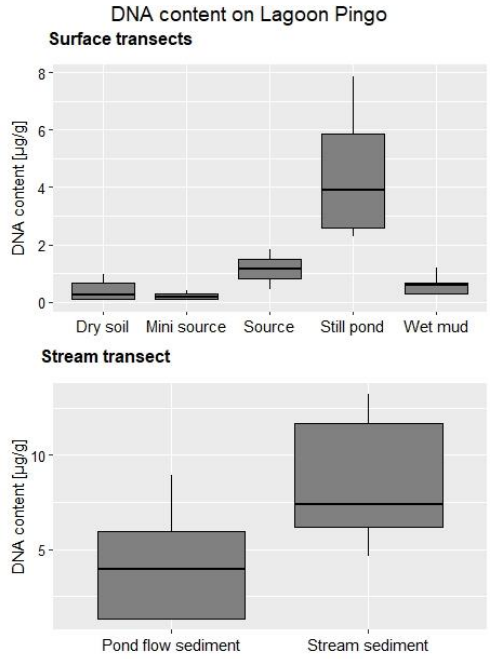

Figure 12: DNA contents on LP according to their category and divided into 'Surface transects' and 'Stream transect'.

The highest average DNA content per g wet sediment was found in the 'Stream sediment' category with an average of 8.6 (± 3.6) µg/g (**Figure 12**). The categories 'Still pond' and 'Pond flow sediment' had approximately equal average DNA contents, with 4.5 (± 2.6) and 4.3 (± 3.2) µg/g, respectively. The 'Source' category had an average of 1 (± 0.7) µg/g. The lowest DNA contents were found in the categories 'Wet mud', 'Dry soil' and 'Mini Source' with averages of 0.6 (± 0.3), 0.4 (± 0.3) and 0.2 (± 0.2) µg/g, respectively. The Kruskal-Wallis test indicated that there were significant differences between the categories (χ^2 =30.11, $p = 3.7 * 10^5$). A one-tailed Student's t-test showed that the 'Stream sediment' category had a significantly higher DNA content than the 'Pond flow sediment' category (t = - 2.035, p = 0.036). Normality was validated using the Shapiro-Wilk test.

3.1.3.2 *pmoA* and 16S abundance

To estimate the number of MOB and of the total prokaryotic population in the sediments, the *pmoA* and 16S abundances were determined for each sampling spot by qPCR (n = 2).

Similarly to the DNA content, the *pmoA* copy numbers of the stream transect were higher on average than the *pmoA* copy numbers of the surface transects (**Figure 13**). However, the difference in *pmoA* copy numbers between the categories 'Pond flow sediment' and 'Stream sediment' was not as pronounced as the difference in DNA contents between these two categories. The highest average copy numbers per g wet sediment of all categories had the 'Stream sediment' category with ~ $3.7 * 10^8$ (± $3.7 * 10^8$) copies/g, followed by the 'Pond flow sediment' category with ~ $3.1 * 10^8$ (± $3.1 * 10^8$) copies/g. However, the averages of 'Pond flow sediment' and 'Stream sediment' were influenced by outliers.

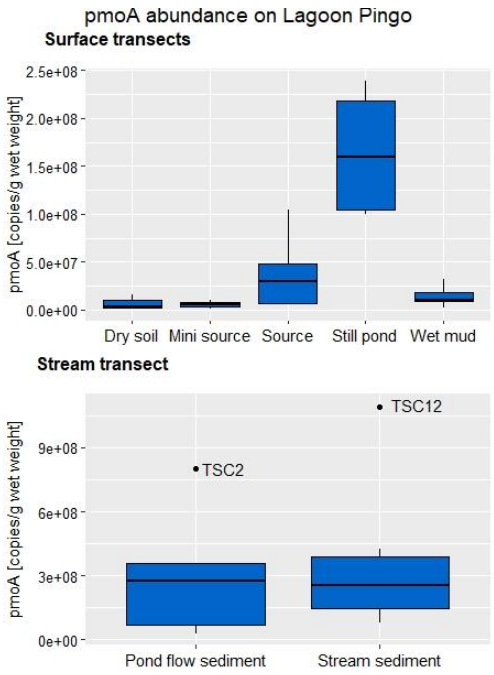

Figure 13*: pmoA* abundance on LP according to their category and divided into 'Surface transects' and 'Stream transect'.

The highest average *pmoA* copy number of the surface transects was found in the 'Still pond' category with an average of ~ $1.6 * 10^8$ ($\pm$ $7.2 * 10^7$) copies/g, whereas the lowest was found in the 'Mini source' category with ~ $5.4 * 10^6$ ($\pm$ $4.6 * 10^6$) copies/g. The categories 'Source', 'Wet mud' and 'Dry soil' had averages of ~ $3.9 * 10^7$ ($\pm$ $4.1 * 10^7$), ~ $1.4 * 10^7$ ($\pm$ $9.6 * 10^6$) and ~ $5.8 * 10^6$ ($\pm$ $5.6 * 10^6$) copies/g, respectively. The Kruskal-Wallis test indicated that there were significant differences between the categories (χ^2 =30.28, p = $3.5 * 10^5$). A two-tailed Student's t-test on square root transformed data showed that there is no significant difference in *pmo*A copy numbers between the 'Stream sediment' and the 'Pond flow sediment' category (t = - 0.39, p = 0.71). Normality was validated using the Shapiro-Wilk test.

The *pmoA* abundances are visualized on the map of LP (**Figure 14**). Average values higher than $2 * 10^8$ *pmoA* copy numbers per g sediment were only found in the stream transect. The source had a lower average *pmoA* copy number per g sediment ($3.9 * 10^7$) than three of the surrounding sampling spots, T1C2 ($2.4 * 10^8$), T2C2 ($1.1 * 10^8$) and TSC2 ($8 * 10^8$). However, the source had a higher average copy number per g sediment than the nearby sampling spot T4C2 ($2.2 * 10^7$). The highest average *pmoA* copy number per gram sediment overall was found

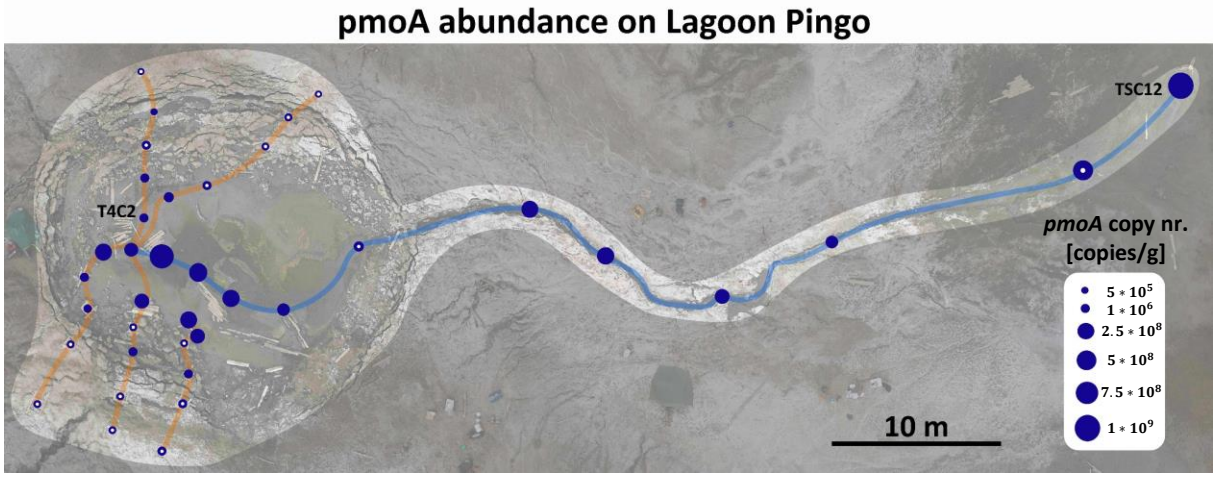

Figure 14*:* Spatial distribution of *pmoA* abundance on LP; the size of the blue circles represents the average copy numbers in copies/g wet weight. A white centre in the blue circles indicates deviating qPCR products, which had a higher melt temperature than expected. For further explanation, the reader is referred to the appendix (p. 64).

at TSC12 ($1.1 * 10^9$), which is furthest from the source, followed by TSC2 ($8 * 10^8$), which is approximately two meters downstream of the source.

The average 16S abundances in the sediment categories (**Figure 15**) exhibited a similarity to the DNA contents of the sediment categories (**Figure 12**). In comparison to the *pmoA* abundances (**Figure 13**), the 16S abundances are not approximately equal in the categories 'Stream sediment' and 'Pond flow sediment', and TSC2 and TSC12 are not statistical outliers of these two categories.

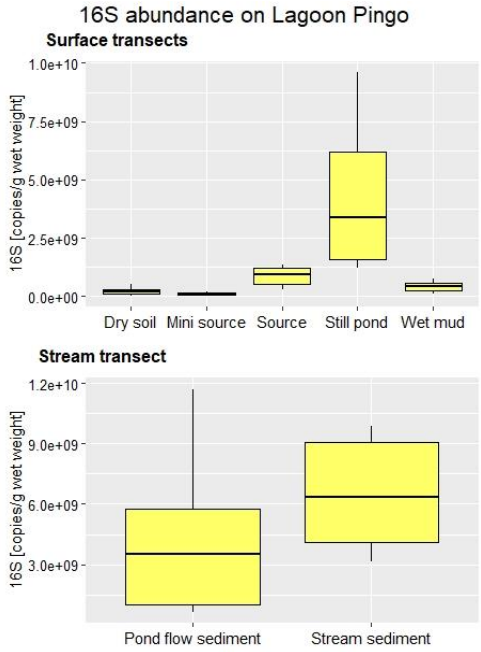

Figure 15: 16S abundance on LP according to their category and divided into 'Surface transects' and 'Stream transect'.

The highest 16S copy number per g sediment was found in the 'Stream sediment' category of the stream transect with $6.5 * 10^9$ ($\pm$ $2.9 * 10^9$) copies/g. In comparison, the 'Pond flow sediment' category had an average of $4.5 * 10^9$ ($\pm$ $4.5 * 10^9$) copies/g. Of the surface transects, the highest average 16S copy numbers per g sediment was found in the 'Still pond' category with $4.4 * 10^9$ ($\pm$ $4.5 * 10^8$) copies/g, followed by the 'Source' sediment category with $8.6 * 10^8$ ($\pm$ $4.5 * 10^8$) copies/g. The categories 'Wet mud', 'Dry soil' and 'Mini source' had copy numbers of $4.2 * 10^8$ ($\pm$ $2.4 * 10^8$), $2.1 * 10^8$ ($\pm$ $1.6 * 10^8$) and $1.1 * 10^8$ ($\pm$ $1 * 10^8$) copies/g, respectively.

A one-tailed Student's t-test showed that there is no significant difference between the 'Stream sediment' and 'Pond flow sediment' categories (t = - 0.88, p = 0.2). Normality was validated using the Shapiro-Wilk test.

3.1.3.3 *pmoA* to 16S copy number ratio

To estimate the dominance of the MOB in the sediment categories, the *pmoA* copy numbers were compared to the 16S copy numbers and calculated as a ratio of *pmoA* to 16S copy numbers. The 'Dry soil' samples could not be amplified appropriately, which had a strong effect on the ratios, and are therefore not shown.

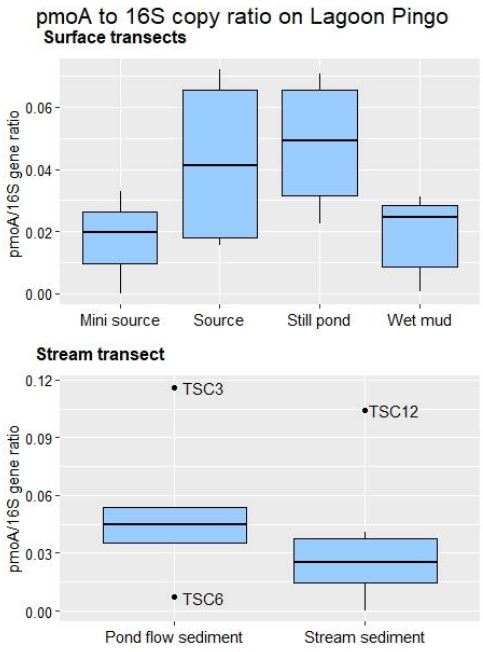

Figure 16: Ratio of *pmoA* to 16S copy numbers on LP according to their category and divided into 'Surface transects' and 'Stream transect'.

In comparison to the *pmoA* and 16S copy numbers per g sediment, the *pmoA* to 16S copy number ratio is rather similar throughout all categories (**Figure 16**). The highest *pmoA* to 16S copy number ratio was found in the category 'Pond flow sediment' with an average of 0.052 (± 0.04). The average ratio of the 'Stream sediment' category was 0.035 (± 0.037 with the large deviation being caused by TSC12). Among the categories of the surface transects, the highest average ratio had the 'Still pond' category with 0.048 (± 0.023), followed by the 'Source', 'Wet mud' and 'Mini source' with 0.042 (± 0.029), 0.019 (± 0.013) and 0.018 (± 0.017), respectively. To test for significant differences between the surface and stream, and between the categories, a two-way ANOVA was performed. Normality and Homogeneity were checked according to the Shapiro-Wilk and Bartlett's test, respectively. The two-way ANOVA results show that there was no significant difference between the surface and the stream [$F(1, 23) = 1.196$, $p = 0.285$) and that there were no significant differences between the categories [$F(4, 23) = 1.233$, $p = 0.324$)].

3.1.4 Pingo 'Stream'

The stream transect generally exhibited higher methane fluxes, oxidation rates, *pmoA* and 16S abundances and DNA contents than the surface transects. The stream stretched from the source towards East, exiting the crater of LP. To identify possible trends, all characteristics (excluding the 16S abundance and the *pmoA* to 16S copy number ratio) of the stream are visualized as a function of the distance to the source in **Figure 17**.

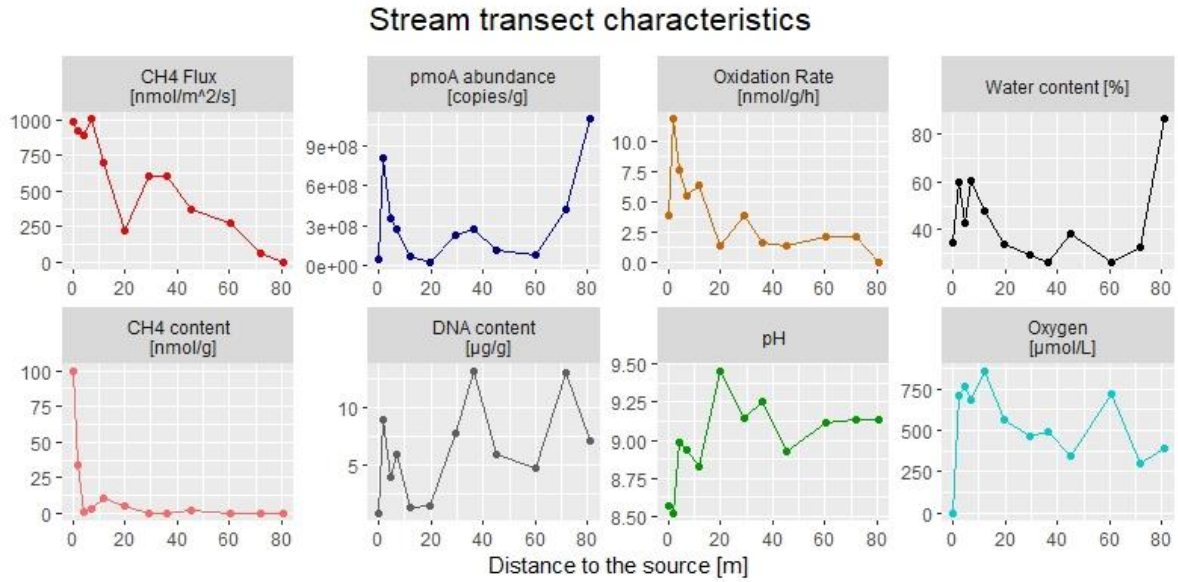

Figure 17: Average characteristics of the stream transect with increasing distance to the source. All points represent the average measured at that distance. The points are connected for the visualization of changes, even though there was no continuous measurement. The x axis label accounts for all graphs. Note the differences in y-axes. Y-axis labels can be found underneath the titles. All sediment weights are given in wet weight.

The methane fluxes exhibited an almost continuously decreasing trend between the first (Source) and last sampling spot in the stream, whereas the sediment methane content decreased to almost 0 nmol/g within the first 4.5 m. The strong decline in the sediment methane content (approx. – 100 nmol/g) was accompanied by the highest methane oxidation rates measured on LP. The oxidation rate decreased towards the end of the stream with one peak at 2 m from the source. At 7 m from the source, the methane flux was the highest of the stream transect, but apart from this, the trend of decreasing methane flux from 0 to 20 m was visible. The source water was anoxic, while the stream water was oxygenated. The pH and the sediment DNA content did not exhibit a consistent pattern throughout the stream. The *pmoA* abundance peaks twice, firstly at 2 m from the source and secondly at the last sampling spot at 80 m from the source (TSC12). However, methane was not oxidized during incubation of sediments from the sampling spot at 80 m (TSC12). The average water content at 80 m was 86 (± 0.3) %.

3.1.5 Linear model analysis

To assess the influence of the environmental parameters on the oxidation rates and *pmoA* abundance, a principle component analysis (PCA) was performed (**Figure 18**). All *pmoA* abundances were kept for further analysis, since amplification problems occurred almost exclusively in the low copy number range.

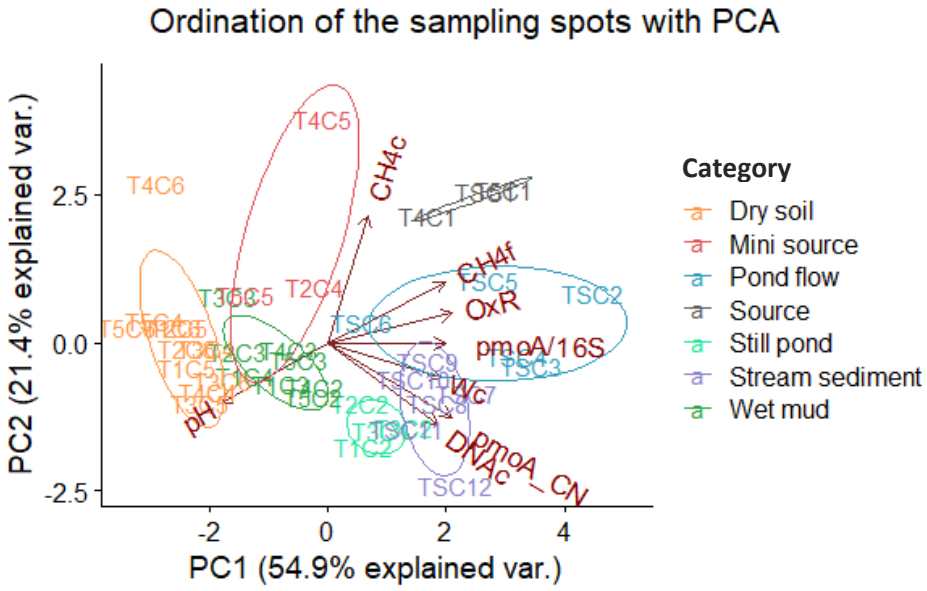

Figure 18: Biplot presenting the first two principle components explaining 76.3 % of the total variance within the dataset; the ordination is presented in scaling 2. Abbreviations: 'c' = content; 'f' = flux; 'CN' = copy numbers; 'Wc' = water content; 'OxR' = oxidation rate.

The categories of the sediment samples clustered with few overlaps (**Figure 18**). Judging from the angles of arrows, the degree of correlation between variables indicated a correlation of the oxidation rate with the methane flux (CH4f) and with the *pmoA* to 16S copy number ratio (pmoA/16S). A correlation between the *pmoA* abundance (pmoA_CN), the DNA content (DNAc) and the water content (Wc) was indicated, while no correlation was indicated between the methane content (CH4c) and the DNA content or the *pmoA* abundance.

To analyse the influences of all environmental parameters on the oxidation rates and *pmoA* abundance of all sampling spots from LP, two forward stepwise multiple regression analyses were performed. The best-fitting model was chosen by the lowest Aikaike information criterion. The best-fitting model for the oxidation rates of the entire pingo was an additive model of the methane flux and the water content. However, the effect of the water content was insignificant [$F(1, 34) = 2.1$; $p = 0.176$]. The second best-fitting model to predict the oxidation rates was based on the methane fluxes alone, but many sampling spots were outside the confidence

interval. No linear model was able to link the *pmoA* abundance to any predictor variable in a meaningful way.

Separate linear regression analyses were performed to relate methane oxidation rates, methane fluxes, and the sediment methane contents to the potential size of the MOB community, represented by the *pmoA* abundance. Additionally, one of the results was compared to the 16S abundance to differentiate possible effects on MOB from effects on the general prokaryotic community. TSC11 was removed from the *pmoA* abundance dataset, due to the uncertainty of the *pmoA* amplification. TSC12 was removed as an outlier due to its frequently observed deviation from the dataset and its great distance from the source (> 80 m).

The linear model of the stream transect showed a significant increase in the oxidation rate with an increase in *pmoA* abundance [$F(1, 8) = 14.687$, $p = 0.005$], which was not the case for the surface transects (**Figure 19 A**). The log-linear model of the oxidation rate as a function of the methane flux predicted a significant positive correlation for the stream transect [$F(1, 9) = 14.111$, $p = 0.0045$], but not for the surface transects (**Figure 19 B**). On the other hand, methane fluxes were not able to predict the *pmoA* abundances (**Figure 19 C**). However, the *pmoA* abundance tended to increase with increasing methane flux in the stream transect even if the model had an R^2 value of 0.24 and a large confidence interval. The sediment methane content was not able to predict the *pmoA* abundance (**Figure 19 D**). The 16S abundance did not show an increase with increasing methane flux (**Figure 19 E**). As a consequence of this lack of effect of the 16S abundance, the *pmoA* to 16S ratio increased together an increase in the methane flux (**Figure 19 F**), even though homoscedasticity was slightly violated (**Table 9**, p. 65)

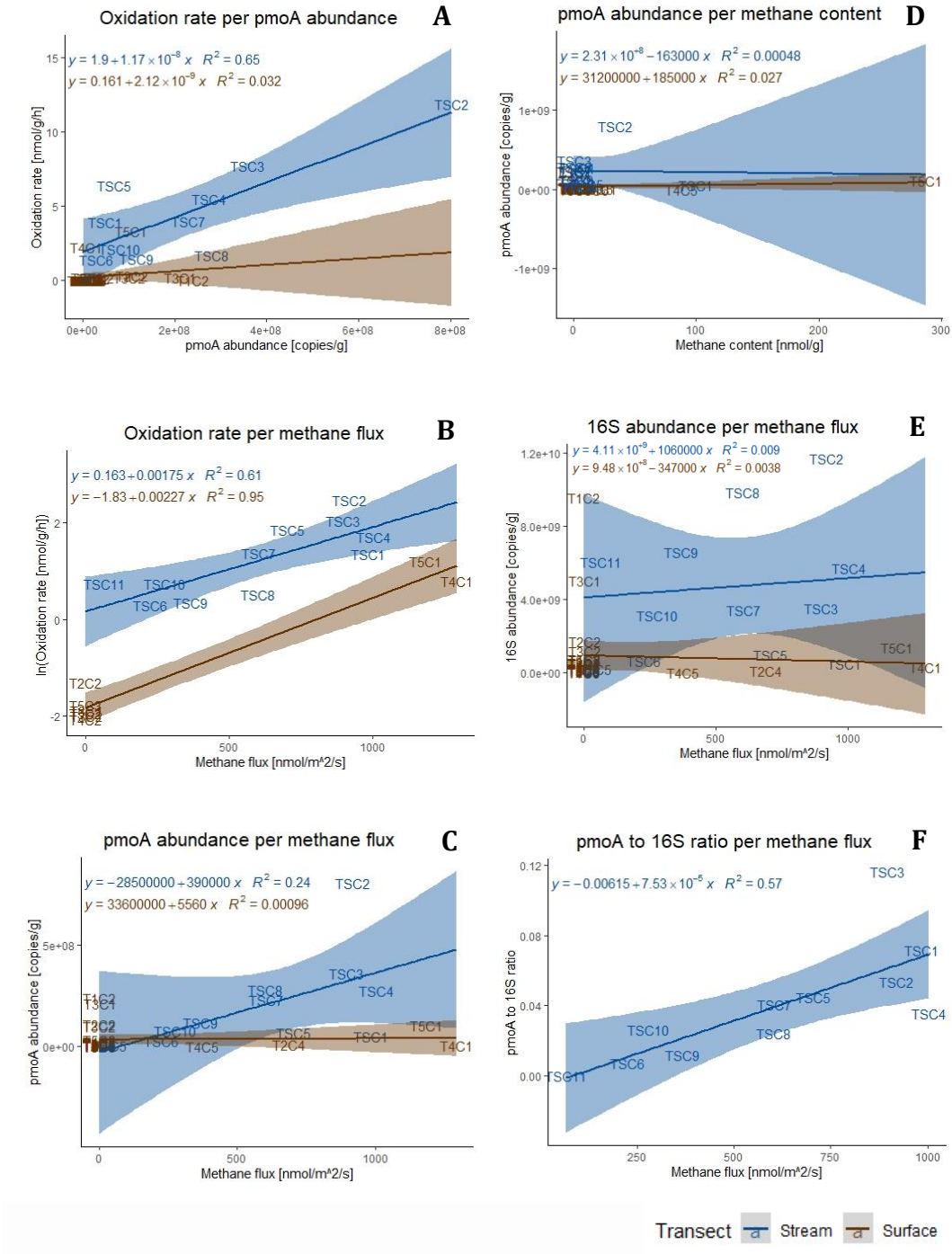

Figure 19: Array of linear regression models. **A** oxidation rate ~ *pmoA* abundance. **B** ln(oxidation rate) ~ methane fluxes; all zero-observations removed. **C** *pmoA* abundance ~ methane flux. **D** *pmoA* abundance ~ methane contents of the sediments. **E** 16S abundance ~ methane flux. **F** *pmoA* dominance ~ methane flux. TSC12 is removed from all datasets. TSC11 is removed from the *pmoA* abundance dataset.

3.2 Enrichment of MOB from Lagoon Pingo

MOB were enriched from three different pingos in Adventdalen, Svalbard, and from all sampling seasons (April, August and October) (**Table 4**). The only environmental sample that was not successfully enriched for MOB, was a water sample from Riverbed pingo (see **Figure 7**) collected in April 2019.

All colonies grew on polycarbonate filters floating on diluted NMS media. No growth in liquid media or on agar plates was observed. From multiple colonies in each culture, *pmoA* was amplified by PCR and sequenced using Sanger sequencing.

Table 4: Overview of enrichment cultures obtained from pingos in Adventdalen. The seasons refer to high Arctic seasons and may differ from seasons elsewhere.

Name	Origin	Sample Type	Season
ELOCT18	Ebullition Lake (beside Lagoon Pingo)	Water	Autumn (October 2018)
LPOCT18	Lagoon Pingo	Snow	Autumn (October 2018)
LPAPR19	Lagoon Pingo	Snow	Spring (April 2019)
IHRAPR19	Innerhytte	Snow	Spring (April 2019)
LPAUG19a	Lagoon Pingo	Sediment	Summer (August 2019)
LPAUG19b	Lagoon Pingo	Sediment	Summer (August 2019)
LPAUG19c	Lagoon Pingo	Sediment	Summer (August 2019)

3.2.1 Molecular characterization

The cultures enriched from three different pingos in Adventdalen were classified on molecular level based on their *pmoA* gene sequences. The best alignments from BLAST searches against the NCBI nucleotide database were with uncultured bacteria, and the MOB species *Methylobacter tundripaludum* (*Gammaproteobacteria*, *Methylococcaceae*).

To phylogenetically place the sequences from the enriched cultures, a minimum evolution tree was constructed incorporating representatives of six genera belonging to the family *Methylococcaceae*, and rooted upon two representatives of the family *Methylocystaceae* (**Figure 20**). Additionally, the four sequences with highest percentage identity retrieved after BLAST search were incorporated. The *pmoA* genes from the pingo cultures made up a novel cluster within *Methylobacter*, being most closely related to *M. tundripaludum*. The closest relatives within the *Methylobacter* genus were a set of environmental sequences that originated from the Canadian high Arctic (GenBank: HM564357.1, HM564374.1, HM564355.1, HM564371.1; Martineau 2010) and from a Tibetan high plateau (GenBank: MH638940.1; Yiang, X. unpublished).

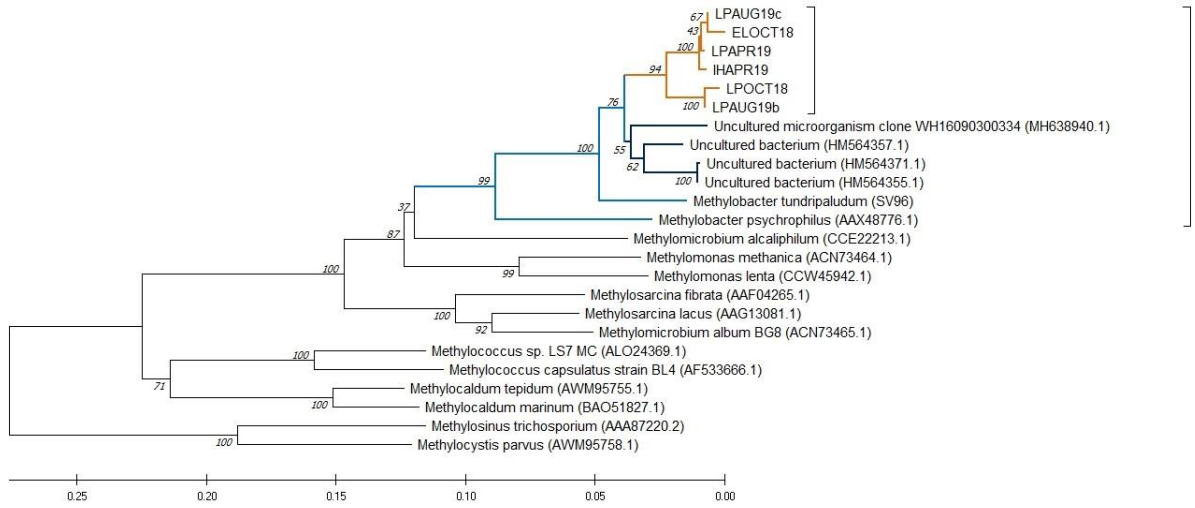

Figure 20: Tree representation of phylogenetic relationships based on *pmoA* sequences using the Minimum Evolution algorithm. The tree is rooted upon the Type II MOB. *Methylocystis parvus* and *Methylosinus trichosporium*. The *Methylobacter* group is highlighted in blue, including the four closest relatives to the enriched sequences (highlighted by a darker blue). The enriched sequences are coloured in orange and combined by a bracket, within a larger bracket (*Methylobacter*). Bootstrap values are shown at the nodes of the tree. The scale bar indicates the estimated phylogenetic divergence.

The phylogenetic distances of the enriched MOB were evaluated with a distance matrix to identify at which taxonomic level the MOB clustered (**Table 5**). According to the distance matrix, the sequences of LPAUG19c, LPAPR19 and IHAPR19 are identical or maximally 0.4 % different. LPAUG19a was distant from all other sequences, with only 60 % sequence

similarity. The average distance between all sequences from the enrichment excluding LPAUG19a was 1.9 %, with the greatest being 5.1 % and the smallest 0 %. Distances to *M. tundripaludum* were on average 7.7 %.

Table 5: Pairwise distance analysis computed by Mega-X with the p-distance model. Increasing sequence similarity is depicted by a colour change from red through yellow to green. The *pmoA* sequence of *Methylobacter tundripaludum* (here: SV96) was used as a reference.

	LPAUG19a	SV96	ELOCT18	LPOCT18	LPAUG19b	LPAUG19c	LPAPR19	IHAPR19
LPAUG19a								
SV96	0.604							
ELOCT18	0.591	0.074						
LPOCT18	0.595	0.087	0.051					
LPAUG19b	0.596	0.081	0.026	0.005				
LPAUG19c	0.595	0.069	0.005	0.025	0.020			
LPAPR19	0.595	0.075	0.024	0.032	0.023	0.000		
IHAPR19	0.595	0.073	0.022	0.027	0.023	0.000	0.004	

The sequence similarities with *M. tundripaludum* were taken from the NCBI BLAST alignment to obtain information on whether the enriched MOB represented a novel species or new *M. tundripaludum* strains (**Table 6**).

Table 6: Sequence similarities to *M. tundripaludum*, the closest cultured and described relative, and the query coverages.

	Percent Identity [%]	Query Coverage [%]
ELOCT18	89.35	100
LPOCT18	90.79	94
IHAPR19	92.92	94
LPAPR19	92.92	94
LPAUG19b	91.10	96
LPAUG19c	92.87	96

Among the enriched cultures, IHAPR19 and LPAPR19 had the smallest sequence dissimilarity of 7.08 % to *M. tundripaludum*, while ELOCT18 had the greatest sequence dissimilarity with 10.65 %. On average, the enriched MOB had a sequence dissimilarity of 8.34 %. The query coverages were between 94 and 100 %.

During the sequence examination, the divergence of the sequence of LPAUG19a to the remaining sequences became apparent. Beside the approx. 40 % difference to the sequence of *M. tundripaludum* (**Table 5**), the sequence of LPAUG19a also showed an approx. 40% difference to the Type II MOB, *Methylosinus trichosporium* and *Methylocystis parvus* (data not shown). Moreover, when aligning the sequence to the NCBI database using the BLAST algorithm, the closest sequence to the one from LPAUG19a lies within the genome assembly of Pseudomonas sp. CC6-YY-74 (GeneBank: CP019947.1). Due to the differences, the sequence of LPAUG19a was not included into the phylogenetic tree or compared to *M. tundripaludum*.

3.2.2 Phenotypical characterization

To distinguish the MOB from contaminants and to determine their morphology, a combination of fluorescence in situ hybridization using a Type-I-MOB specific probe (MG-64) and light microscopy was used.

Most cells, indicated by the DAPI stain, showed a double staining (DAPI and probe) in the merged picture when the EUB338 probe was used, except for the negative control (**Figure 21**). The only two enrichment cultures showing positive staining with the MG-64 probe were LPAUG19c and IHAPR19 (**Figure 22**). The remaining enrichment cultures appeared like LPOCT18, in which only DAPI and EUB338 signals were visible, and therefore, only LPOCT18 is shown (**Figure 21** and **Figure 22**). However, cells stained with DAPI, but unstained with the MG-64 probe were visible in the enrichment culture LPAUG19c. These cells generally appeared smaller than the MG-64 stained cells. Cells of IHAPR19 aggregated strongly and were sparsely distributed. In comparison, LPAUG19c exhibited a high cell density and a more even distribution. Therefore, LPAUG19c was used to determine the cellular morphology of the MOB (**Figure 23**). The cell length and width were measured on light microscopy pictures.

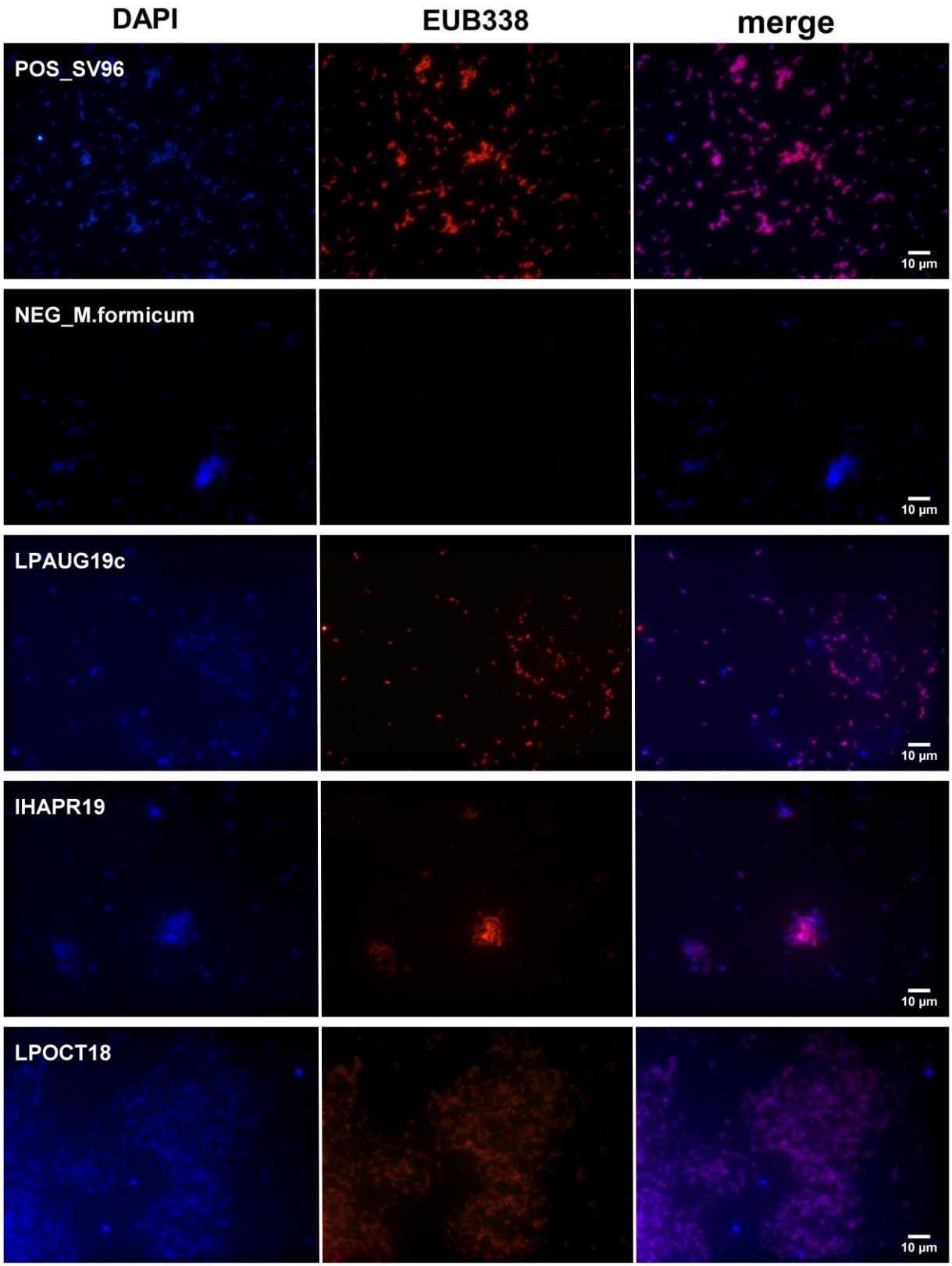

Figure 21: Cells stained with the probe EUB338 and DAPI. The DAPI signal is presented in the left column; the probe signal is presented in the central column and the merged picture is presented in the column to the left. In merged picture: Cells stained with the bacterial EUB338 probe and DAPI appear in purple, DAPI only in blue and the probes' signal only appears in red. Signal intensities are not a comparable due to varying exposure times.

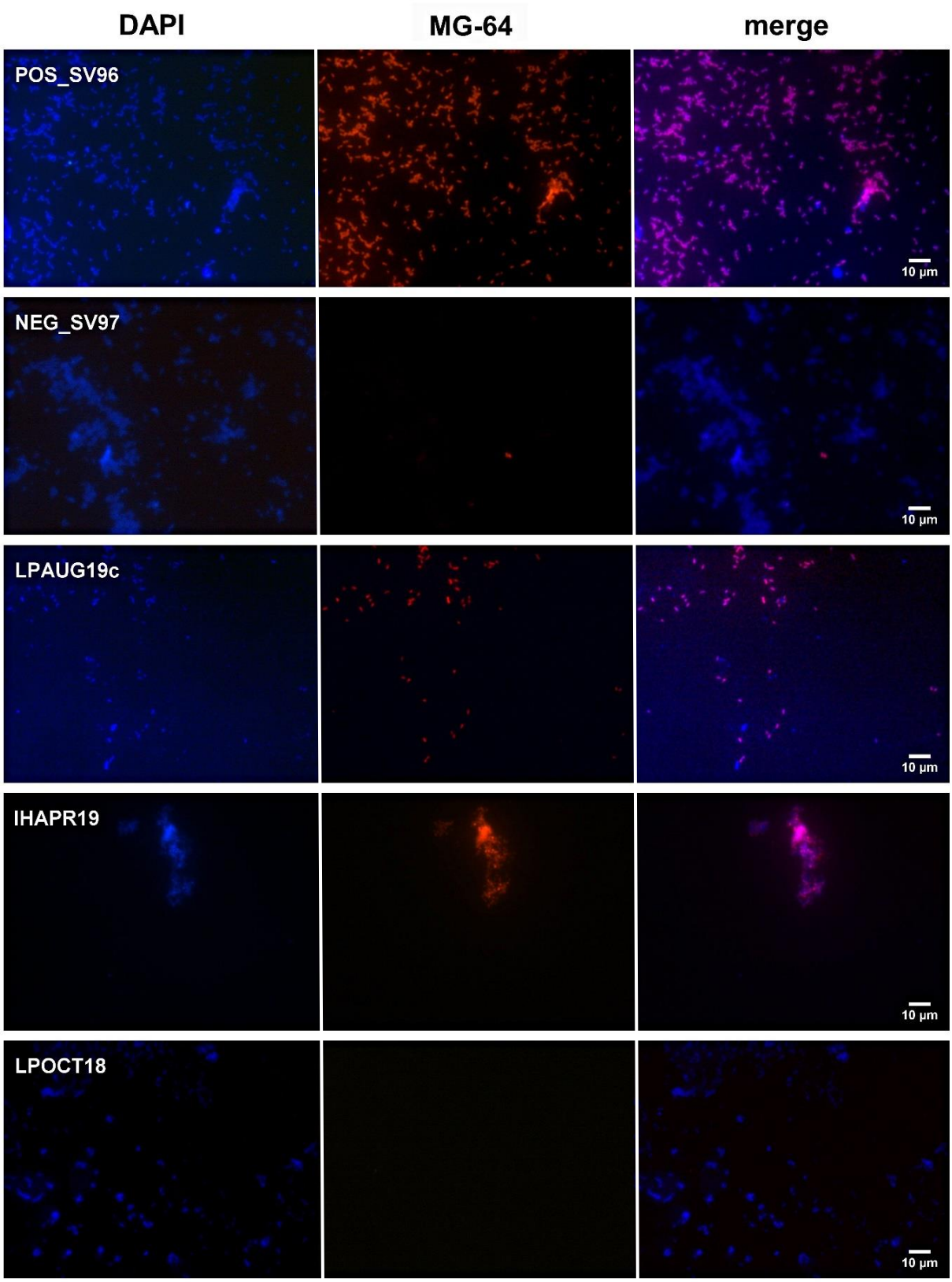

Figure 22: Cells stained with the probe MG-64 and DAPI. Arrangement as in Fig. 23. In merged picture: Cells stained with the Type-I-MOB-specific probe and DAPI appear in purple, DAPI only in blue and the probes' signal only appears in red. Signal intensities are not a comparable due to varying exposure times.

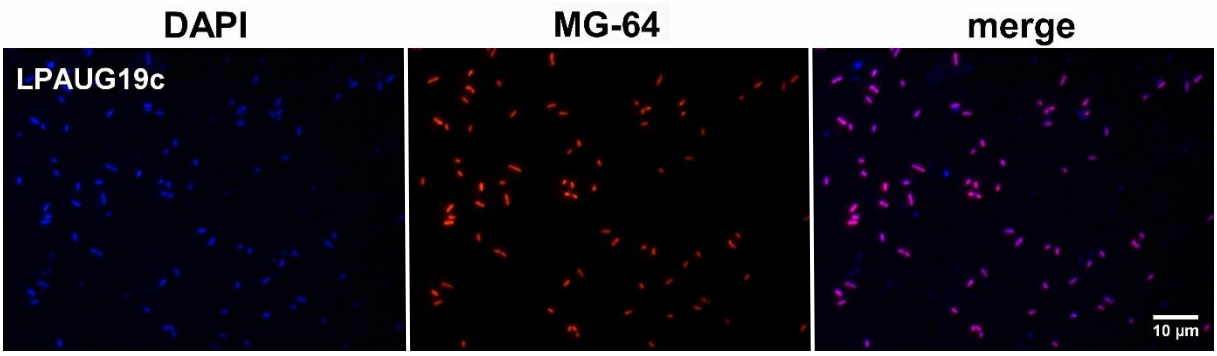

Figure 23: Cells of the enrichment LPAUG19c stained with DAPI and MG-64. Cells appearing purple in the merged picture were defined as methanotrophic.

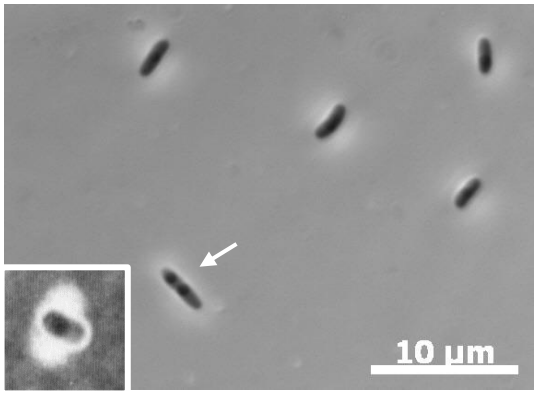

Figure 24: LPAUG19c MOB. Pictures taken using phase contrast microscopy. An image of a germinated spore of *Methylosinus trichosporium* (Whittenbury et al. 1970a) is given at the bottom left for comparison reasons

The MOB in the LPAUG19c enrichment had a rod-shaped cell morphology with a length ranging from ~ 1.6 to ~ 3.3 µm and a width of ~0.6 to ~0.9 µm. Motility was not observed. Round and darker shapes were observed within the cells, resembling the spores of *Methylosinus trichosporium* (Whittenbury et al., 1970a). The shapes were located in various positions within the cells, and the observed maximum was twice within one cell (**Figure 24**, white arrow). Possible spore germination steps, as described for *M. trichosporium* by Whittenbury et al., were observed (**Figure 25**). Other cell morphologies than the rod-shaped cells labelled with the MG-64 probe were identified within the LPAUG19c enrichment using light microscopy (not shown).

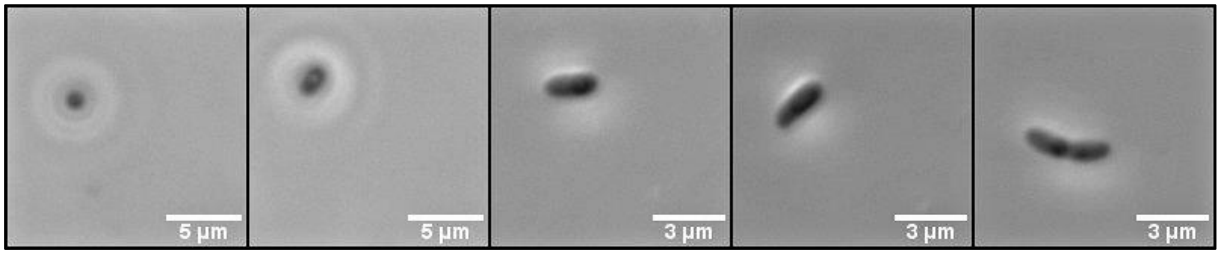

Figure 25: Possible germination of exospores observed in LPAUG19c using phase contrast microscopy

4 Discussion

4.1 Methane oxidizing bacteria on Lagoon Pingo

4.1.1 Methane fluxes

Methane flux measurements on LP have shown that the methane evasion is not limited to one specific source and its discharge in late summer, which confirms the first hypothesis. However, the information gained represents a snapshot and does not necessarily apply for an extended period of time. All fluxes represented in this thesis are net fluxes, which might be composed as described in the following equation. Inferences about the composition of the fluxes cannot be drawn at this point.

$$Net\ CH_4\ flux = thermogenic\ CH_4 + biogenic\ CH_4 - CH_4\ oxidation$$

The methane fluxes measured on LP were strikingly high in comparison to natural methane emitting landscapes, such as the Siberian permafrost from the Lena Delta which had an average methane flux of ~ 140 µmol/m^2/h (Wagner et al., 2003) or wetland soils from West Greenland, which emitted on average 14 µmol/m^2/h (Christiansen et al., 2015). For example, the main source of LP emitted on average ~ 4806 µmol/m^2/h and the miniature source T2C4 emitted on average 2470 µmol/m^2/h. However, as described in the introduction, LP may be classified as a terrestrial methane seep and should therefore be compared to such. Following the definitions by Etiope et al. mentioned in the introduction, LP may be categorized as a water seep, since methane is discharged with water through the main source (Etiope et al., 2009a). If the definitions by Spulber et al. 2010 for seepage-types on mud volcanoes were applied to the pingo structure, the source and most of the stream water surfaces, as well as two out of three miniature sources, can be classified as miniseepage (~ $2.6 * 10^3$ µmol/m^2/h). Two sampling spots, the miniature source T5C5 and the end stream transect sampling spot TSC11 are in the range of microseepage (~ 26 to 260 µmol/m^2/h). The methane fluxes of the remaining methane emitting sampling spots are below of the seepage-types defined by Spulber et al. No methane flux measured on LP was in the magnitude of macro-seeps (~ $2.6 * 10^6$ µmol/m^2/h) (Spulber et al., 2010). However, categorizing LP in zones with different flux intensities as proposed by Hong et al. might be advantageous, since the stream is not a stationary system (Hong et al., 2013).

The highest methane fluxes were measured above the source, followed by the water surfaces of the close surroundings of which the flux intensity generally decreased with increasing distance to the source. This, combined with the fact that methane was consistently detected in the water

(data not shown), suggests that the main source is the predominant methane supplier of the system and the water released through the source is its carrier. However, whether or not the main source is the only methane supplier to the water remains uncertain, as contradicting observations were made along the stream, e.g., low methane fluxes followed by higher methane fluxes (see **Figure 9** and **Figure 17**). Therefore, undetected sources may further supply the pond and stream. It also remains uncertain whether methane only diffuses from the water into the underlying sediment or if the sediment also percolates methane from underneath and thereby contributes to the methane fluxes.

However, methane fluxes were also measured from the sediment surfaces of the surface transects, albeit with lower intensities in comparison to the water surface. Among these sediment surfaces, those closest to the pond and the so-called miniature sources exhibited the highest methane fluxes. These findings raise the question of the origin of the methane emitted from the sediment surfaces.

One explanation may be that the pore water of the sediments of LP trap methane while being covered with water from the source and release it during summer. It has been shown before, that soils of different properties store and emit methane to different degrees. Of the soil types tested in a study by Wang et al., clay soils trapped and stored most methane (Wang et al., 1993). The sediments of the 'Wet mud' category, found close to the pond area, might resemble clayey soils. During summer, when warmer temperatures result in a retracting water coverage, the entrapped methane would be emitted during the following drying process, similar to how it can be observed for fallow rice fields. However, the methane trapped in fallow rice fields was generally released within 12 days (Fitzgerald et al., 2000, Neue et al., 1996). Therefore, this explanation would most likely not hold for the entire summer season on LP.

Another explanation may be that methane is present or produced underneath the pond area. Following this, the different surfaces could represent membranes with different porosities for the ascending methane, hampering the methane fluxes to different degrees. According to Hong et al. 2013, wet mud may even depict an "impermeable cover to gas", which can decrease methane fluxes on mud volcanoes (Hong et al. 2013, p. 7). Cracks in the sediment layers (as seen in **Figure 30**, appendix p. 65), would allow direct water and gas transport to the surface, and may hereby increase the methane flux. However, Hong et al. also point out, that the surface conditions do not necessarily represent the subsurface conditions, which further complicates interpretations. Contrarily, the observation of ebullition from waterlogged mud, could indicate

that methane is percolating through the sediments. A summary of the scenario described in the second explanation is depicted in **Figure 26**, which is based on a figure by Hodson et al. 2019 that suggested the location of ice is right underneath the pond. The conjecture by Yoshikawa and Koichiro 1995 that there is gas underneath the pingo supports this scenario. However, the two explanations given in this discussion do not contradict each other and might both be valid.

4.1.2 Oxidation rates

The incubation experiments brought important insight into the methane oxidation potential on LP. Firstly, the parallel incubation of stream water and sediment from the exact same sampling spots revealed that, at least under the given incubation conditions, the water does not oxidize methane, whereas the sediment does. However, whether methanotrophs are present in the water, which may oxidize methane under different (e.g. anoxic) conditions, remains unanswered. Since the incubation temperature was chosen to resemble the Arctic summer, it is likely that the sediments on site oxidize methane during the summer season. Moreover, within the data obtained in this thesis, the methane oxidation rates of the pond and stream sediment seem to be positively correlated to the methane fluxes. The methane fluxes, even though influenced by microbial oxidation, are possibly predicting the methane availability to the MOB.

However, even though it seemed reasonable to inject the bottles with two different amounts of methane, as described in chapter 2.2.2, it made it impossible to compare between the groups of the surface transect, or the pingo surface transects and the stream transect. According to the Michaelis-Menten kinetics, the enzyme rate depends on the substrate availability: $v_0 = v_{max} \frac{[S]}{K_m + [S]}$; in which v_0 is the enzymatic reaction rate, v_{max} is the maximal reaction rate, $[S]$ is the substrate concentration, and K_m is the Michaelis constant. For high substrate concentrations, this term becomes independent of the substrate, and the enzymatic reaction rate is highest. In conclusion, the observed differences in methane oxidation rates do not automatically represent quantitative differences in oxidation potential. The oxidation experiments rather show where MOB are present and possibly active in the sediments of LP. That the oxidation potential is not necessarily different between the sediment categories as shown in **Figure 11**, is supported by the finding of similar *pmoA* copy numbers in the 'Still pond' sediment category and the stream transect categories. However, the *pmoA* copy numbers based on DNA do not automatically relate to the *in situ* activity (see 4.1.3). Exceptional is the 'Dry soil' category, which neither exhibited oxidation nor had high *pmoA* copy numbers. This may be due to the distance to the pond water. If the water is the only carrier of methane, the

‘Dry soil’ does not encounter the substrate needed to establish a methanotrophic community and subsequently an oxidation potential. Possible loci of *in situ* methane oxidation on LP are indicated in **Figure 26**.

The incubations of sediments from the sampling spot TSC12 did not exhibit methane oxidation, despite the high abundance of *pmoA*. The high *pmoA* abundance is unlikely an experimental error, as a high *Methylobacter* sequence abundance was also observed in the 16S sequencing analysis by the master’s student Pernille Fåne. However, the water content of the sediment used for the incubations was at an average of 86 %. Incubation experiments have shown that oxidation rates generally decrease with a water content above 50 % (Czepiel et al., 1995, Yang and Chang, 1998), although none of these studies incubated soils with a water content as high as 86 %. Methane oxidation may have been limited by methane diffusion, and possibly blurred with methane production if oxygen diffusion was limited due to the high water content. Therefore, it remains unsure if sediments from TSC12 possess the potential to oxidize methane. To clearly resolve whether or not samples with high water contents have the potential to oxidize methane, the water content could have been adjusted as performed by Nesbit and Breitenbeck (Nesbit and Breitenbeck, 1992).

Overall, the sampling spot TSC12 seems to differ from all other sampling spots, which may be explained in two ways. Firstly, since TSC12 is located at the end of the stream, the high *pmoA* abundance may be from cells that are washed up by the stream. In that case, the cells may not have the potential to oxidize methane anymore, since they would not be supplied with methane by the stream, shown by the absence of a significant methane flux. Secondly, the sampling spot may resemble a typical permafrost habitat, in which the MOB of the active layer are supplied with methane from methanogenesis (Barbier et al., 2012).

4.1.3 *pmoA* abundance and dominance

The *pmoA* abundances found on LP (not including TSC12, see explanation in 4.1.2) range from $\sim 5 * 10^5$ *pmoA* copies/g wet sediment in the dry periphery of the pingo, to $\sim 8 * 10^8$ *pmoA* copies g wet sediment in the sediments two meters apart from the main source (TSC2). These numbers are generally higher than reported for other permafrost environments. In a permafrost (thermokarst) pond in northern Norway $\sim 4 * 10^8$ *pmoA* copies were found in the upper soil layers per dry weight (Liebner et al., 2015). However, this number will decrease if it is calculated per wet weight, and will possibly be in the range of 10^4 and 10^6 *pmoA* copies/g dry weight, as found in the upper permafrost layer of the Canadian Arctic (Frank-Fahle et al., 2014).

On the other hand, a study on MOB in a Tibetan wetland, which used the same primer set for qPCR amplifications as used in this thesis, found comparable copy numbers of ~ $3.7 * 10^8$ per gram wet weight (Yun et al., 2012). Considering that LP represents a so far undescribed habitat-type, which seems to be fuelled by methane-saturated water, the higher *pmoA* copy numbers of this thesis in comparison to other permafrost studies may be reasonable.

qPCR amplifications of the *pmoA* gene from almost all sediments of the 'Dry soil' category resulted in products with higher melt temperatures. Possibly, a low concentration of the targeted gene could have coerced the amplification of unspecific products, which differ in length or GC content and therefore show a higher melt temperature. The problem of deviating product sizes when amplifying *pmoA* with a qPCR approach may be a common problem, as it was observed multiple times before with different primer sets [(Bodelier et al., 2009, Freitag et al., 2010); Bodelier at al. 2009: Appendix S1]. Furthermore, low amplification efficiencies (78.8 %) were also observed in a study by Christiansen et al., even though another reverse primer was used in their study (Christiansen et al., 2016). Many other studies applying the Kolb et al. 2003 qPCR protocol (including modified versions) do not mention the amplification efficiency or do not give exact numbers (Bodelier et al., 2009, Yun et al., 2012, Knief et al., 2006, Martineau et al., 2010). However, as a result, the ratio of MOB in comparison to the entire bacterial population is expected to be underestimated, due to the imbalance between the amplification efficiencies in this thesis (*pmoA* ~ 80% and 16S ~ 100%).

Since the copy numbers of the 16S rRNA genes per genome vary strongly between different bacterial species and *pmoA* has been found in several copies per MOB genome, the copy numbers obtained in this thesis were not used to estimate total cell number (Dunfield et al., 2007, Semrau et al., 1995, Vetrovsky and Baldrian, 2013). Therefore, a stronger MOB dominance was simply inferred from a comparably higher *pmoA* to 16S copy number ratio. However, the insignificant differences in the *pmoA* to 16S copy number ratio between the sediment categories indicate that MOB do not clearly dominate stronger in any sediment category of LP.

The ratio of *pmoA* to 16S copy numbers found in this thesis ranged from 0 to 0.12. These ratios deviate strongly from the ratios found in other environments. They deviate drastically from the numbers that were obtained from methane oxidizing forest soils (Christiansen et al., 2016) of which the highest average ratio was 0.0026. In the thermokarst pond from Northern Norway mentioned above, the highest *pmoA* to total bacterial 16S copy number ratio found was 0.016

(Liebner et al., 2015). Even though neither study directly calculated the *pmoA* to 16S copy number ratio, average copy numbers were given. Therefore, an approximation of their *pmoA* to 16S copy number ratio could be calculated. A study on Russian permafrost soils found MOB to total bacteria ratios of up to 0.26, which is approximately in the range of the ratios found in this thesis (Liebner and Wagner, 2007). However, the Liebner and Wagner permafrost study quantified the cell numbers microscopically and aimed therefore cellular numbers and not gene copy numbers.

When the sediment categories are compared, the highest *pmoA* abundances were found in the 'Still pond' category, and the stream transect categories 'Pond flow sediment' and 'Stream sediment'. Each of these categories is covered with water that originated from the source. In comparison, sediments from the 'Dry soil' category had low *pmoA* abundances and were not in contact with water from the source. The tendency of the *pmoA* abundance to correlate with the oxidation rate, supports the reasoning that the oxidation observed is due to the MOB community present in the sediments. This was corroborated by a weak positive correlation between the *pmoA* to 16S copy number ratio and the methane flux in the stream transect. The methane fluxes, possibly indicating the provision of the MOB with substrate, may reinforce the dominance of the methanotrophic bacteria in comparison to the general bacterial population. However, the insignificant differences in *pmoA* dominance between the sediment categories indicated that even if methane fluxes promote the MOB community, it does not significantly affect the relative abundance of MOB. This might even indicate that the methane is directly or indirectly fuelling large parts of the community. The 'Stream sediment' category may be an exception to this as the average microbial biomass (as indicated by the DNA content) was significantly higher than in the 'Pond flow sediment' category, despite the methane fluxes, the *pmoA* copy numbers and *pmoA* to 16S copy number ratio being lower.

Nevertheless, the *pmoA* abundance is only estimating the size of the MOB community on LP, including active and inactive cells. Inferences about their *in situ* activity cannot be directly drawn from the abundances. The Yun et al. 2012 study examining the abundance and activity of *pmoA* from *Methylobacter* and *Methylocystis* in a Tibetan wetland, found *Methylobacter* to be more abundant, but less active than *Methylocystis* (Yun et al., 2012). Moreover, in a study on methane oxidation in peat bogs in Wales, no linear relationship was found between the methane fluxes and the bare *pmoA* abundance, while a trend was observed using the gene:transcript ratio (Freitag et al., 2010). This example further supports the importance of including transcript data when analysing *in situ* methane oxidation on a molecular level.

However, within the aims of this thesis, to prove the existence of MOB on LP and link their presence to methane availability, the application of qPCR on DNA was sufficient.

4.1.4 Miniature sources

The scenario introduced in chapter 4.1.1, that methane is rising from underneath the pingo through the surfaces, could also explain the existence of the so-called miniature sources, which seemed spatially unrelated to the water emitted from the main source. Within the scenario, the miniature sources represent highly permeable areas, with a less impeded transit of the methane into the atmosphere. The absence of methane oxidation matched the low *pmoA* copy numbers, indicating an inability of the miniature sources to function as a habitat for MOB. The overall low DNA content and 16S abundance in the miniature sources may further demonstrate their inhabitability in comparison with all other sediment categories. However, it is at this point not excluded, that the miniature source harbour small archaeal communities able to oxidize methane anaerobically, which would make them a micro-habitat comparable to mud volcanoes.

4.1.5 Methanotrophy on Lagoon Pingo

The results obtained within this thesis show the existence of MOB on LP and thus verifies the second hypothesis to be true. Moreover, the gene necessary for aerobic methane oxidation was found widely distributed in sediments of LP that were in contact with water from the source. Even though the activity patterns of MOB *in situ* are not fully explored, it is likely that the observed rates of methane oxidation depict which sediment possess the potential for methane oxidation. Additionally, it was shown that the sediments possess the potential to oxidize methane under the given conditions, whereas the water does not. However, whether methanotrophs are present in the water remains to be answered.

According to the third hypothesis, the methane content of the sediment can represent the methane availability and predict the presence of MOB (by *pmoA* gene abundance). This was not confirmed. Therefore, the hypothesis must be rejected. Contrarily, within the data obtained, the methane fluxes were estimated to be the best predictor for methane oxidation. Moreover, in the stream, the methane oxidation potential seems to relate exponentially to the methane fluxes. Therefore, it may be hypothesized that the methane fluxes represent methane availability and can thus be used to predict the methane oxidation potential for the stream. However, the methane fluxes are measured at the surface of the water and the *pmoA* abundance was detected within the sediments underneath the water. Therefore, the methane fluxes are presumably

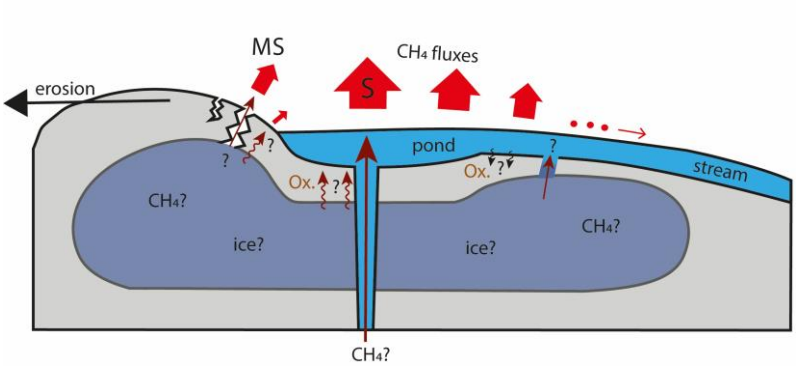

Figure 26: Possible explanation scheme for the methane fluxes and oxidation observed on LP during the fieldwork in August 2019. The figure is adapted from **Hodson et al (2019)**. Wide red arrows = methane fluxes. Thin dark red arrows = possible gas emergence pathways. Black arrows = possible diffusion into the sediment. The S indicates the main source, whereas MS indicates the miniature sources. Ox. Indicates possible in situ oxidation. Question marks indicate uncertainties.

proportionally representing the methane content in the water, which also diffuses into the sediment. On the other hand, the depiction of the sediment methane contents of the stream transect, as a function of the distance to the source, as shown in **Figure 17**, raises the question whether the decline of methane in the sediments within the first 4.5 m was due to methanotrophic oxidation. The structure of Lagoon Pingo as a habitat for MOB as it may be proposed from the data of this thesis, combined with all proposed methane flux origins is presented in **Figure 26**.

4.2 Enrichment of MOB from Lagoon Pingo

Psychrotolerant MOB were successfully enriched from three different Adventdalen pingos, although none of the enriched MOB (**Table 4**) were observed as a pure culture. This conclusion was underpinned by three observations: a) spreading the culture on sugar-rich media agar plates incubated with only atmospheric methane available, always resulted in the growth of colonies with one or more morphologies; b) light microscopy revealed more than one cell morphology; c) Sanger Sequencing of the 16S rRNA gene did not yield readable sequences. Absence of growth on sugar-rich media is a generally accepted method to indicate the purity of a MOB culture, since no MOB has been successfully cultivated on sugar-rich media so-far (Rhee et al., 2019, Svenning et al., 2003).

4.2.1 Description of *Methylobacter* sp.

Relying on the 4% species cut-off value for *pmoA* sequences suggested by Knief 2015, it can be inferred that the MOB obtained from the enrichment cultures all belong to the same novel undescribed species within the genus Methylobacter (Knief, 2015). However, this inference should additionally be verified with 16S rRNA gene sequences.

Table 7: Comparison of the Methylobacter species found on Adventdalen pingos to the type strain of the closest relative, *M. tundripaludum*, based on preliminary indications. Question marks depict uncertainties.

Characteristic	*LP19*	*SV96* ^{T}
Rod-shaped cells	+	+
Length	1.6 - 3.3 µm	1.9 - 2.5 µm
Width	0.6 - 0.9 µm	0.8 - 1.3 µm
Colony pigmentation	- (?)	+
Cyst or spore formation	+ (?)	-
NaCl tolerance	+	-
High pH (~9) tolerance	+	-
Broad temp. tolerance	+	+
Psychrophily	-	-

Within the cluster of the novel *Methylobacter* species, the sequences LPAUG19c, LPAPR19 and IHAPR19 were almost identical (> 99.5% sequence identity) and do not represent different strains. Neither are LPAUG19b and LPOCT18 (99.5% sequence identity). LPAUG19a is possibly a *Pseudomonas* strain and might have been wrongly associated with MOB. The sequence obtained possibly encodes an ammonia monooxygenase, which is related to the methane monooxygenase and can occur in *Pseudomonas* strains (Holmes et al., 1995, Zhang et al., 2011). The sequence of ELOCT18 shows many ambiguous bases, which could be due to the presence of several *pmoA* sequences in a mixed culture. In conclusion, the number of enriched clones of the novel *Methylobacter* sp. is lowered down to two strains. The terms species, strain and clone are used according the definitions provided by Dijkshoorn et al. (Dijkshoorn et al., 2000). However, since only MOB were successfully stained with a Type-I-MOB specific probe in LPAUG19c and IHAPR19 cultures, all remaining strains were possibly lost during isolation attempts. Staining failures of the remaining strains are unlikely, since the EUB338 probe successfully stained nearly all cells in every culture. Successful staining with the EUB338 probe provides transferable information about the hybridization efficiency of the MG-64 probe, since both probes are of similar size and composition. Non-specific staining of the EUB338 probe seems unlikely, but cannot be excluded since no test using the complementary probe called NON338 was performed (Manz et al., 1992).

The novel *Methylobacter* species, named *Methylobacter* sp. LP19, is rod-shaped with an average length of 2.4 µm and average width of 0.7 µm. The clone possesses areas of high refractive indices, appearing round and dark in phase contrast microscopy. These are presumably resting stages in the form of exospores, since observations were made, which resemble the germination of *M. trichosporium* spores (Whittenbury et al., 1970a). Resting stages in *Methylobacter* were described as cysts resembling those found in *Azotobacter* (Bowman et al., 1993, Whittenbury et al., 1970a), which differ from the ones observed in *M.* sp. LP19. Alternatively, the observations could be storage granules. Under starvation, some

MOB store carbon in inclusions, commonly poly-β-hydroxybutyrate (PHB), which due to the high refractive index can appear dark when observed through a phase contrast microscope. The formation of such storage inclusions can be triggered by nitrogen limitation (Whittenbury et al., 1970b), and the characteristics presented in **Figure 24** resemble PHB inclusions within *M. trichosporium* under nitrogen-limitation (Xin et al., 2007). However, the ability of Type I MOB to produce PHB storage compounds has not been proven beyond doubt [reviewed in (Pieja et al., 2011)]. Moreover, *M. trichosporium* is a Type II MOB and therefore a very distant relative to the *Methylobacter* genus. In conclusion, observations between *M. trichosporium* and *M.* sp. LP19 should not be compared without questioning, especially since neither exospores nor PHB inclusions were proven before within a *Methylobacter* species (Collins et al., 2017).

4.2.2 *Methylobacter* sp. on Adventdalen pingos

The novel *Methylobacter* sp. LP19 was enriched several times from pingo structures in the Adventdalen valley, the clone from Lagoon Pingo being identical to the clone of the Innerhytte pingo, further up the valley. Nevertheless, these occurrences do not necessarily imply that this species is common to all pingos or that it is limitedly occurring on pingos.

The dark features observed with light microscopy, may be an adaptation to the environment suiting either explanation, that the features are resting stages or storage granules. If the species develops resting stages, it may be an adaptation to the strong seasonal changes and the cold temperatures on Svalbard as proposed by Trotsenko and Khmelenina, 2005. If the species develops storage granules, it may be an adaptation to store carbon compounds for periods of starvation. Either case might be necessary to survive the winter in which the water underneath the ice lid becomes anoxic (Hodson et al., 2019). The species may benefit from such adaptations to changing environments, which possibly enables it to outcompete other species. Even though it is not verified that the enriched species is the dominant species on LP, it is nevertheless likely. A low diversity of the methanotrophic community with few active species was suggested before for another Arctic environment, peat soil (Graef et al., 2011), and the repeatedly enrichment of the same species that exhibits great adaptation skills from different seasons supports this suggestion. Whether or not the species is the dominant active species in situ and not only the most easily enrichable species, could be tested with metatranscriptomic studies on RNA.

4.2.3 Significance and outlook of the enrichment

Overall, the enrichment and characterization of a novel MOB is of considerable scientific significance. Particularly if it is shown to be a dominant member of methane seep communities,

significantly affecting methane emissions from these systems. The full description of a novel species would improve the quality of metagenomics and metatranscriptomic approaches by providing a reference, but also broaden the understanding of MOB phylogeny and biogeography. The finding of either PHB granules or exospores would further describe the range of adaptations to which *Methylobacter* species are capable. Moreover, an isolated species that can tolerate greatly fluctuating temperature, salt and oxygen concentrations could greatly contribute to biotechnological applications. However, in order to enable these applications, isolation needs to be pursued further, followed by an in-depth characterization of the species.

5 Conclusions

Within this thesis it has been shown that methane is seeping in various positions on Lagoon Pingo and that the water is the main carrier of methane. Beside the main source, miniature sources were shown to exist as areas of high methane ebullition. Moreover, methano oxidizing bacteria were shown to exist on Lagoon Pingo. However, since water has been shown to most likely not oxidize methane, the aerobic microbial mitigation on Lagoon Pingo seems limited. However, in case the methane is percolating through the sediment from a larger source underneath, the mitigation of the aerobic microbial community may have a large effect on the contribution of Lagoon Pingo to local methane emissions.

6 Outlook

This thesis has successfully laid the foundation for further in-depth research about the methanotrophic community on Lagoon Pingo by giving evidence with several methods that MOB are present. It is worth pursuing the further isolation of the psychrotolerant MOB from Lagoon Pingo to better understand the local organisms, and for enabling possible bioprospecting or biotechnological applications. The investigation of Lagoon Pingo's ecological importance will be continued in several consecutive fieldwork campaigns and the associated laboratory work. During this investigation, it is important to test to what extent the MOB are active in the field and how much they mitigate methane emissions, by for example reverse-transcriptase qPCR or metatranscriptomic studies. Higher temperature incubation experiments may help understanding how the system will adapt to climate change and see whether the oxidation potential can possibly increase with temperature. Moreover, to better understand the methane fluxes on Lagoon Pingo, it may be helpful to determine the origin of the gas and test whether it is oxidized by ANME even before reaching the surface.

Literature

ALAIN, K., HOLLER, T., MUSAT, F., ELVERT, M., TREUDE, T. & KRUGER, M. 2006. Microbiological investigation of methane- and hydrocarbon-discharging mud volcanoes in the Carpathian Mountains, Romania. *Environ Microbiol,* 8**,** 574-90.

AMANN, R. I., BINDER, B. J., OLSON, R. J., CHISHOLM, S. W., DEVEREUX, R. & STAHL, D. A. 1990. Combination of 16S rRNA-targeted oligonucleotide probes with flow cytometry for analyzing mixed microbial populations. *Appl Environ Microbiol,* 56**,** 1919-25.

ANGEL, R., CLAUS, P. & CONRAD, R. 2012. Methanogenic archaea are globally ubiquitous in aerated soils and become active under wet anoxic conditions. *ISME J,* 6**,** 847-62.

ANTHONY, K. M. W., ANTHONY, P., GROSSE, G. & CHANTON, J. 2012. Geologic methane seeps along boundaries of Arctic permafrost thaw and melting glaciers. *Nature Geoscience,* 5**,** 419-426.

BARBIER, B. A., DZIDUCH, I., LIEBNER, S., GANZERT, L., LANTUIT, H., POLLARD, W. & WAGNER, D. 2012. Methane-cycling communities in a permafrost-affected soil on Herschel Island, Western Canadian Arctic: active layer profiling of mcrA and pmoA genes. *FEMS Microbiol Ecol,* 82**,** 287-302.

BELOVA, S. E., OSHKIN, I. Y., GLAGOLEV, M. V., LAPSHINA, E. D., MAKSYUTOV, S. S. & DEDYSH, S. N. 2014. Methanotrophic bacteria in cold seeps of the floodplains of northern rivers. *Microbiology,* 82**,** 743-750.

BENNIKE, O. 1998. Pingos at Nioghalvfjerdsfjorden, eastern North Greenland. *Geology of Greenland Survey Bulletin,* 180**,** 159-162.

BODELIER, P. L., KAMST, M., MEIMA-FRANKE, M., STRALIS-PAVESE, N. & BODROSSY, L. 2009. Whole-community genome amplification (WCGA) leads to compositional bias in methane-oxidizing communities as assessed by pmoA-based microarray analyses and QPCR. *Environ Microbiol Rep,* 1**,** 434-41.

BORCARD, D., GILLET, F. & LEGENDRE, P. 2011. *Cluster Analysis,* New York, NY, New York, NY: Springer New York.

BORCARD, D., GILLET, F. & LEGENDRE, P. 2018. *Numerical Ecology with R,* Cham, Springer International Publishing, Cham.

BOURNE, D. G., HOLMES, A. J., IVERSEN, N. & MURRELL, J. C. 2000. Fluorescent oligonucleotide rDNA probes for specific detection of methane oxidising bacteria. *FEMS Microbiol Ecol,* 31**,** 29-38.

BOWLES, M. W., SAMARKIN, V. A., HUNTER, K. S., FINKE, N., TESKE, A. P., GIRGUIS, P. R. & JOYE, S. B. 2019. Remarkable Capacity for Anaerobic Oxidation of Methane at High Methane Concentration. *Geophysical Research Letters,* 46**,** 12192-12201.

BOWMAN, J. P. 2015. Methylocystaceae fam. nov. *Bergey's Manual of Systematics of Archaea and Bacteria.*

BOWMAN, J. P. 2016. Methylococcaceae. *Bergey's Manual of Systematics of Archaea and Bacteria.*

BOWMAN, J. P., MCCAMMON, S. A. & SKERRATT, J. H. 1997. Methylosphaera hansonii gen. nov., sp. nov., a psychropholic, group I methanotroph from Antarctic marine-salinity, meromictic lake. *Microbiology,* 143**,** 1451-1459.

BOWMAN, J. P., SLY, L. I., NICHOLS, P. D. & HAYWARD, A. C. 1993. Revised Taxonomy of the Methanotrophs: Description of Methylobacter gen. nov., Emendation of Methylococcus, Validation of Methylosinus and Methylocystis Species, and a Proposal that the Family Methylococcaceae Includes Only the Group I Methanotrophs. *International Journal of Systematic Bacteriology,* 43**,** 735-753.

BURCHETT, W. W., ELLIS, A. R., HARRAR, S. W. & BATHKE, A. C. 2017. Nonparametric Inference for Multivariate Data: The R Package npmv. *2017,* 76**,** 18.

BURROWS, K. J., CORNISH, A., SCOTT, D. & HIGGINS, I. J. 1984. Substrate specificities of the soluble and particulate methane mono-oxygenases of Methylosinus trichosporium OB3b. *Microbiology,* 130**,** 3327-3333.

CHAN, O. C., CLAUS, P., CASPER, P., ULRICH, A., LUEDERS, T. & CONRAD, R. 2005. Vertical distribution of structure and function of the methanogenic archaeal community in Lake Dagow sediment. *Environ Microbiol,* 7**,** 1139-49.

CHENG, T. W., CHANG, Y. H., TANG, S. L., TSENG, C. H., CHIANG, P. W., CHANG, K. T., SUN, C. H., CHEN, Y. G., KUO, H. C., WANG, C. H., CHU, P. H., SONG, S. R., WANG, P. L. & LIN, L. H. 2012. Metabolic stratification driven by surface and subsurface interactions in a terrestrial mud volcano. *ISME J,* 6**,** 2280-90.

CHRISTIANSEN, J. R., LEVY-BOOTH, D., PRESCOTT, C. E. & GRAYSTON, S. J. 2016. Microbial and Environmental Controls of Methane Fluxes Along a Soil Moisture Gradient in a Pacific Coastal Temperate Rainforest. *Ecosystems,* 19**,** 1255-1270.

CHRISTIANSEN, J. R., ROMERO, A. J. B., JØRGENSEN, N. O. G., GLARING, M. A., JØRGENSEN, C. J., BERG, L. K. & ELBERLING, B. 2015. Methane fluxes and the functional groups of methanotrophs and methanogens in a young Arctic landscape on Disko Island, West Greenland. *Biogeochemistry,* 122**,** 15-33.

COLLETT, T. S., LEE, M. W., AGENA, W. F., MILLER, J. J., LEWIS, K. A., ZYRIANOVA, M. V., BOSWELL, R. & INKS, T. L. 2011. Permafrost-associated natural gas hydrate occurrences on the Alaska North Slope. *Marine and Petroleum Geology,* 28**,** 279-294.

COLLINS, D. A., AKBERDIN, I. R. & KALYUZHNAYA, M. G. 2017. Methylobacter. *Bergey's Manual of Systematics of Archaea and Bacteria.*

COSTELLO, A. M. & LIDSTROM, M. E. 1999. Molecular characterization of functional and phylogenetic genes from natural populations of methanotrophs in lake sediments. *Appl Environ Microbiol,* 65**,** 5066-74.

CZEPIEL, P. M., CRILL, P. M. & HARRISS, R. C. 1995. Environmental factors influencing the variability of methane oxidation in temperate zone soils. *Journal of Geophysical Research: Atmospheres,* 100**,** 9359-9364.

DAMM, E., MACKENSEN, A., BUDÉUS, G., FABER, E. & HANFLAND, C. 2005. Pathways of methane in seawater: Plume spreading in an Arctic shelf environment (SW-Spitsbergen). *Continental Shelf Research,* 25**,** 1453-1472.

DAVIES, S. L. & WHITTENBURY, R. 1970. Fine structure of methane and other hydrocarbon-utilizing bacteria. *J Gen Microbiol,* 61**,** 227-32.

DENG, Y., CUI, X. & DUMONT, M. G. 2016. Identification of active aerobic methanotrophs in plateau wetlands using DNA stable isotope probing. *FEMS Microbiol Lett,* 363.

DIJKSHOORN, L., URSING, B. M. & URSING, J. B. 2000. Strain, clone and species: comments on three basic concepts of bacteriology. *J Med Microbiol,* 49**,** 397-401.

DIMITROV, L. I. 2002. Mud volcanoes - the most important pathway for degassing deeply buried sediments. *Earth-Science Reviews,* 59**,** 49-76.

DUNFIELD, P. F., KHMELENINA, V. N., SUZINA, N. E., TROTSENKO, Y. A. & DEDYSH, S. N. 2003. Methylocella silvestris sp. nov., a novel methanotroph isolated from an acidic forest cambisol. *Int J Syst Evol Microbiol,* 53**,** 1231-9.

DUNFIELD, P. F., YURYEV, A., SENIN, P., SMIRNOVA, A. V., STOTT, M. B., HOU, S., LY, B., SAW, J. H., ZHOU, Z., REN, Y., WANG, J., MOUNTAIN, B. W., CROWE, M. A., WEATHERBY, T. M., BODELIER, P. L., LIESACK, W., FENG, L., WANG, L. & ALAM, M. 2007. Methane oxidation by an extremely acidophilic bacterium of the phylum Verrucomicrobia. *Nature,* 450**,** 879-82.

ETIOPE, G., FEYZULLAYEV, A. & BACIU, C. L. 2009a. Terrestrial methane seeps and mud volcanoes: A global perspective of gas origin. *Marine and Petroleum Geology,* 26**,** 333-344.

ETIOPE, G., FEYZULLAYEV, A., MILKOV, A. V., WASEDA, A., MIZOBE, K. & SUN, C. H. 2009b. Evidence of subsurface anaerobic biodegradation of hydrocarbons and potential secondary methanogenesis in terrestrial mud volcanoes. *Marine and Petroleum Geology,* 26**,** 1692-1703.

ETIOPE, G. & MILKOV, A. V. 2004. A new estimate of global methane flux from onshore and shallow submarine mud volcanoes to the atmosphere. *Environmental Geology,* 46**,** 997-1002.

ETIOPE, G., NAKADA, R., TANAKA, K. & YOSHIDA, N. 2011. Gas seepage from Tokamachi mud volcanoes, onshore Niigata Basin (Japan): Origin, post-genetic alterations and CH4–CO2 fluxes. *Applied Geochemistry,* 26**,** 348-359.

ETTWIG, K. F., BUTLER, M. K., LE PASLIER, D., PELLETIER, E., MANGENOT, S., KUYPERS, M. M., SCHREIBER, F., DUTILH, B. E., ZEDELIUS, J., DE BEER, D., GLOERICH, J., WESSELS, H. J., VAN ALEN, T., LUESKEN, F., WU, M. L., VAN DE PAS-SCHOONEN, K. T., OP DEN CAMP, H. J., JANSSEN-MEGENS, E. M., FRANCOIJS, K. J., STUNNENBERG, H., WEISSENBACH, J., JETTEN, M. S. & STROUS, M. 2010. Nitrite-driven anaerobic methane oxidation by oxygenic bacteria. *Nature,* 464**,** 543-8.

FITZGERALD, G., SCOW, K., HILL, J. & FITZGERALD, G. 2000. Fallow season straw and water management effects on methane emissions in California rice. *Global Biogeochemical Cycles,* 14**,** 767-776.

FORWICK, M., BAETEN, N. J. & VORREN, T. O. Pockmarks in Spitsbergen fjords. *Norwegian Journal of Geology,* 89**,** 65 - 77.

FOX, J. & WEISBERG, S. 2019. An R Companion to Applied Regression (Third). Thousand Oaks CA: Sage.

FRANK-FAHLE, B. A., YERGEAU, E., GREER, C. W., LANTUIT, H. & WAGNER, D. 2014. Microbial functional potential and community composition in permafrost-affected soils of the NW Canadian Arctic. *PLoS One,* 9**,** e84761.

FREITAG, T. E., TOET, S., INESON, P. & PROSSER, J. I. 2010. Links between methane flux and transcriptional activities of methanogens and methane oxidizers in a blanket peat bog. *FEMS Microbiol Ecol,* 73**,** 157-65.

GILBERT, G. L., O'NEILL, H. B., NEMEC, W., THIEL, C., CHRISTIANSEN, H. H., BUYLAERT, J.-P. & EYLES, N. 2018. Late Quaternary sedimentation and permafrost development in a Svalbard fjord-valley, Norwegian high Arctic. *Sedimentology,* 65**,** 2531-2558.

GONZALEZ-VALENCIA, R., MAGANA-RODRIGUEZ, F., GERARDO-NIETO, O., SEPULVEDA-JAUREGUI, A., MARTINEZ-CRUZ, K., ANTHONY, K. W., BAER, D. & THALASSO, F. 2014. In situ measurement of dissolved methane and carbon dioxide in freshwater ecosystems by off-axis integrated cavity output spectroscopy. *Environ Sci Technol,* 48**,** 11421-8.

GRAEF, C., HESTNES, A. G., SVENNING, M. M. & FRENZEL, P. 2011. The active methanotrophic community in a wetland from the High Arctic. *Environ Microbiol Rep,* 3**,** 466-72.

GURNEY, S. D. 1998. Aspects of the genesis and geomorphology of pingos: Perennial permafrost mounds. *Progress in Physical Geography,* 22**,** 307-324.

HANSON, R. S. & HANSON, T. E. 1996. Methanotrophic Bacteria. *Microbiological Reviews,* 60**,** 439-471.

HE, R., WOOLLER, M. J., POHLMAN, J. W., QUENSEN, J., TIEDJE, J. M. & LEIGH, M. B. 2012. Diversity of active aerobic methanotrophs along depth profiles of arctic and subarctic lake water column and sediments. *ISME J,* 6**,** 1937-48.

HENCKEL, T., FRIEDRICH, M. & CONRAD, R. 1999. Molecular analyses of the methane-oxidizing microbial community in rice field soil by targeting the genes of the 16S rRNA, particulate methane monooxygenase, and methanol dehydrogenase. *Appl Environ Microbiol,* 65**,** 1980-90.

HJELLE, A. 1993. *Geology of Spitzbergen,* Polarhåndbok No. 7, Norsk Polarinstitutt, Oslo.

HODSON, A., NOWAK, A., REDEKER, K. R., HOLMLUND, E. S., CHRISTIANSEN, H. H. & TURCHYN, A. V. 2019. Seasonal Dynamics of Methane and Carbon Dioxide Evasion From an Open System Pingo: Lagoon Pingo, Svalbard. *Frontiers in Earth Science,* 7**,** 1 - 12.

HODSON, A. J., NOWAK, A., SENGER, K., REDEKER, K., CHRISTIANSEN, H. H., JESSEN, S., HORNUM, M. T., BETLEM, P., THORNTON, S. F., TURCHYN, A. V., OLAUSSEN, S. & MARCA, A. 2020. Open system pingos as hotspots for sub-permafrost methane emission in Svalbard. *The Cryosphere Discuss.,* 2020**,** 1-21.

HOLMES, A. J., COSTELLO, A., LIDSTROM, M. E. & MURRELL, J. C. 1995. Evidence That Particulate Methane Monooxygenase and Ammonia Monooxygenase May Be Evolutionarily Related. *Fems Microbiology Letters,* 132**,** 203-208.

HONG, W.-L., ETIOPE, G., YANG, T. F. & CHANG, P.-Y. 2013. Methane flux from miniseepage in mud volcanoes of SW Taiwan: Comparison with the data from Italy, Romania, and Azerbaijan. *Journal of Asian Earth Sciences,* 65**,** 3-12.

HOVLAND, M., GARDNER, J. V. & JUDD, A. G. 2002. The significance of pockmarks to understanding fluid flow processes and geohazards. *Geofluids,* 2**,** 127-136.

ISAKSEN, I. S. A., GAUSS, M., MYHRE, G., WALTER ANTHONY, K. M. & RUPPEL, C. 2011. Strong atmospheric chemistry feedback to climate warming from Arctic methane emissions. *Global Biogeochemical Cycles,* 25**,** n/a-n/a.

JIANG, H., CHEN, Y., JIANG, P., ZHANG, C., SMITH, T. J., MURRELL, J. C. & XING, X.-H. 2010. Methanotrophs: Multifunctional bacteria with promising applications in environmental bioengineering. *Biochemical Engineering Journal,* 49**,** 277-288.

KALYUZHNAYA, M. G., KHMELENINA, V., ESHINIMAEV, B., SOROKIN, D., FUSE, H., LIDSTROM, M. & TROTSENKO, Y. 2008. Classification of halo(alkali)philic and halo(alkali)tolerant methanotrophs provisionally assigned to the genera Methylomicrobium and Methylobacter and emended description of the genus Methylomicrobium. *Int J Syst Evol Microbiol,* 58**,** 591-6.

KHADEM, A. F., POL, A., WIECZOREK, A., MOHAMMADI, S. S., FRANCOIJS, K. J., STUNNENBERG, H. G., JETTEN, M. S. & OP DEN CAMP, H. J. 2011. Autotrophic methanotrophy in verrucomicrobia: Methylacidiphilum fumariolicum SolV uses the Calvin-Benson-Bassham cycle for carbon dioxide fixation. *J Bacteriol,* 193**,** 4438-46.

KHMELENINA, V. N., KALYUZHNAYA, M. G., SAKHAROVSKY, V. G., SUZINA, N. E., TROTSENKO, Y. A. & GOTTSCHALK, G. 1999. Osmoadaptation in halophilic and alkaliphilic methanotrophs. *Arch Microbiol,* 172**,** 321-9.

KITS, K. D., KLOTZ, M. G. & STEIN, L. Y. 2015. Methane oxidation coupled to nitrate reduction under hypoxia by the Gammaproteobacterium Methylomonas denitrificans, sp. nov. type strain FJG1. *Environ Microbiol,* 17**,** 3219-32.

KNIEF, C. 2015. Diversity and Habitat Preferences of Cultivated and Uncultivated Aerobic Methanotrophic Bacteria Evaluated Based on pmoA as Molecular Marker. *Front Microbiol,* 6**,** 1346.

KNIEF, C., KOLB, S., BODELIER, P. L., LIPSKI, A. & DUNFIELD, P. F. 2006. The active methanotrophic community in hydromorphic soils changes in response to changing methane concentration. *Environ Microbiol,* 8**,** 321-33.

KNITTEL, K. & BOETIUS, A. 2009. Anaerobic Oxidation of Methane: Progress with an Unknown Process. *Annual Review of Microbiology,* 63**,** 311-334.

KOLB, S., KNIEF, C., STUBNER, S. & CONRAD, R. 2003. Quantitative detection of methanotrophs in soil by novel pmoA-targeted real-time PCR assays. *Appl Environ Microbiol,* 69**,** 2423-9.

KOTELNIKOVA, S. 2002. Microbial production and oxidation of methane in deep subsurface. *Earth-Science Reviews,* 58**,** 367-395.

KUMAR S., STECHER G., M., L., C., K. & K., T. 2018. MEGA X: Molecular Evolutionary Genetics Analysis across computing platforms. *Molecular Biology and Evolution,* 35**,** 1547-1549.

LIEBNER, S., GANZERT, L., KISS, A., YANG, S., WAGNER, D. & SVENNING, M. M. 2015. Shifts in methanogenic community composition and methane fluxes along the degradation of discontinuous permafrost. *Front Microbiol,* 6**,** 356.

LIEBNER, S. & WAGNER, D. 2007. Abundance, distribution and potential activity of methane oxidizing bacteria in permafrost soils from the Lena Delta, Siberia. *Environ Microbiol,* 9**,** 107-17.

MACKAY, J. R. 1998. Pingo Growth and collapse, Tuktoyaktuk Peninsula Area, Western Arctic Coast, Canada: a long-term field study. *Géographie physique et Quaternaire,* 52**,** 269-396.

MAGEN, C., LAPHAM, L. L., POHLMAN, J. W., MARSHALL, K., BOSMAN, S., CASSO, M. & CHANTON, J. P. 2014. A simple headspace equilibration method for measuring dissolved methane. *Limnology and Oceanography: Methods,* 12**,** 637-650.

MANZ, W., AMANN, R., LUDWIG, W., WAGNER, M. & SCHLEIFER, K.-H. 1992. Phylogenetic Oligodeoxynucleotide Probes for the Major Subclasses of Proteobacteria: Problems and Solutions. *Systematic and Applied Microbiology,* 15**,** 593-600.

MARÍN-MORENO, H., GIUSTINIANI, M., TINIVELLA, U. & PIÑERO, E. 2016. The challenges of quantifying the carbon stored in Arctic marine gas hydrate. *Marine and Petroleum Geology,* 71**,** 76-82.

MARTINEAU, C., WHYTE, L. G. & GREER, C. W. 2010. Stable isotope probing analysis of the diversity and activity of methanotrophic bacteria in soils from the Canadian high Arctic. *Appl Environ Microbiol,* 76**,** 5773-84.

MCCALLEY, C. K., WOODCROFT, B. J., HODGKINS, S. B., WEHR, R. A., KIM, E.-H., MONDAV, R., CRILL, P. M., CHANTON, J. P., RICH, V. I. & TYSON, G. W. 2014. Methane dynamics regulated by microbial community response to permafrost thaw. *Nature,* 514**,** 478-481.

MCDONALD, I. R., BODROSSY, L., CHEN, Y. & MURRELL, J. C. 2008. Molecular ecology techniques for the study of aerobic methanotrophs. *Appl Environ Microbiol,* 74**,** 1305-15.

MILKOV, A. V. 2000. Worldwide distribution of submarine mud volcanoes and associated gas hydrates. *Marine Geology,* 167**,** 29-42.

NESBIT, S. P. & BREITENBECK, G. A. 1992. A laboratory study of factors influencing methane uptake by soils. *Agriculture, Ecosystems and Environment,* 41**,** 39 - 54.

NEUE, H. U., WASSMANN, R., LANTIN, R. S., ALBERTO, M. C. R., ADUNA, J. B. & JAVELLANA, A. M. 1996. Factors affecting methane emission from rice fields. *Atmospheric Environment,* 30**,** 1751-1754.

NIEDERBERGER, T. D., PERREAULT, N. N., TILLE, S., LOLLAR, B. S., LACRAMPE-COULOUME, G., ANDERSEN, D., GREER, C. W., POLLARD, W. & WHYTE, L. G. 2010. Microbial characterization of a subzero, hypersaline methane seep in the Canadian High Arctic. *ISME J,* 4**,** 1326-39.

OMEL'CHENKO, M. V., VASIL'EVA, L. V., ZAVARZIN, G. A., SAVEL'EVA, N. D., LYSENKO, A. M., MITYUSHINA, L. L., KHMELENINA, V. N. & TROTSENKO, Y. A. 1996. A novel psychrophilic methanotroph of the genus Methylobacter. *Microbiology (New York, NY),* 65**,** 339-343.

OP DEN CAMP, H. J., ISLAM, T., STOTT, M. B., HARHANGI, H. R., HYNES, A., SCHOUTEN, S., JETTEN, M. S., BIRKELAND, N. K., POL, A. & DUNFIELD, P. F. 2009. Environmental, genomic and taxonomic perspectives on methanotrophic Verrucomicrobia. *Environ Microbiol Rep,* 1**,** 293-306.

PAULL, C. K., USSLER, W., DALLIMORE, S. R., BLASCO, S. M., LORENSON, T. D., MELLING, H., MEDIOLI, B. E., NIXON, F. M. & MCLAUGHLIN, F. A. 2007. Origin of pingo-like features on the Beaufort Sea shelf and their possible relationship to decomposing methane gas hydrates. *Geophysical Research Letters,* 34.

PIEJA, A. J., ROSTKOWSKI, K. H. & CRIDDLE, C. S. 2011. Distribution and selection of poly-3-hydroxybutyrate production capacity in methanotrophic proteobacteria. *Microb Ecol,* 62**,** 564-73.

PORTNOV, A., VADAKKEPULIYAMBATTA, S., MIENERT, J. & HUBBARD, A. 2016. Ice-sheet-driven methane storage and release in the Arctic. *Nat Commun,* 7**,** 10314.

RAGHOEBARSING, A. A., POL, A., VAN DE PAS-SCHOONEN, K. T., SMOLDERS, A. J., ETTWIG, K. F., RIJPSTRA, W. I., SCHOUTEN, S., DAMSTE, J. S., OP DEN CAMP, H. J., JETTEN, M. S. & STROUS, M. 2006. A microbial consortium couples anaerobic methane oxidation to denitrification. *Nature,* 440**,** 918-21.

REEBURGH, W. S. 2007. Oceanic methane biogeochemistry. *Chem Rev,* 107**,** 486-513.

RHEE, S.-K., AWALA, S. I. & NGUYEN, N.-L. 2019. Enrichment and Isolation of Aerobic and Anaerobic Methanotrophs. *In:* LEE, E. Y. (ed.) *Methanotrophs: Microbiology Fundamentals and Biotechnological Applications.* Cham: Springer International Publishing.

ROSS, N., BRABHAM, P. J., HARRIS, C. & CHRISTIANSEN, H. H. 2007. Internal structure of open system pingos, Adventdalen, Svalbard: The use of resistivity tomography to assess ground-ice conditions. *Journal of Environmental and Engineering Geophysics,* 12**,** 113-126.

RZHETSKY, A. & NEI, M. 1993. Theoretical foundation of the minimum-evolution method of phylogenetic inference. *Mol Biol Evol,* 10**,** 1073-95.

SAMSONOV, S. V., LANTZ, T. C., KOKELJ, S. V. & ZHANG, Y. 2016. Growth of a young pingo in the Canadian Arctic observed by RADARSAT-2 interferometric satellite radar. *The Cryosphere,* 10**,** 799-810.

SCHINDELIN, J., ARGANDA-CARRERAS, I., FRISE, E., KAYNIG, V., LONGAIR, M., PIETZSCH, T., PREIBISCH, S., RUEDEN, C., SAALFELD, S., SCHMID, B., TINEVEZ, J. Y., WHITE, D. J., HARTENSTEIN, V., ELICEIRI, K., TOMANCAK, P. & CARDONA, A. 2012. Fiji: an open-source platform for biological-image analysis. *Nat Methods,* 9**,** 676-82.

SCHÜTZ, H., SCHRÖDER, P. & RENNENBERG, H. 1991. 2 - Role of Plants in Regulating the Methane Flux to the Atmosphere. *In:* SHARKEY, T. D., HOLLAND, E. A. & MOONEY, H. A. (eds.) *Trace Gas Emissions by Plants.* San Diego: Academic Press.

SCHUUR, E. A., MCGUIRE, A. D., SCHADEL, C., GROSSE, G., HARDEN, J. W., HAYES, D. J., HUGELIUS, G., KOVEN, C. D., KUHRY, P., LAWRENCE, D. M., NATALI, S. M., OLEFELDT, D., ROMANOVSKY, V. E., SCHAEFER, K., TURETSKY, M. R., TREAT, C. C. & VONK, J. E. 2015. Climate change and the permafrost carbon feedback. *Nature,* 520**,** 171-9.

SEMRAU, J. D., CHISTOSERDOV, A., LEBRON, J., COSTELLO, A., DAVAGNINO, J., KENNA, E., HOLMES, A. J., FINCH, R., MURRELL, J. C. & LIDSTROM, M. E. 1995. Particulate methane monooxygenase genes in methanotrophs. *J Bacteriol,* 177**,** 3071-9.

SEMRAU, J. D., DISPIRITO, A. A. & YOON, S. 2010. Methanotrophs and copper. *FEMS Microbiology Reviews,* 34**,** 496-531.

SKENNERTON, C. T., WARD, L. M., MICHEL, A., METCALFE, K., VALIENTE, C., MULLIN, S., CHAN, K. Y., GRADINARU, V. & ORPHAN, V. J. 2015. Genomic Reconstruction of an Uncultured Hydrothermal Vent Gammaproteobacterial Methanotroph (Family Methylothermaceae) Indicates Multiple Adaptations to Oxygen Limitation. *Frontiers in Microbiology,* 6**,** 1425.

SMITH, G. J., ANGLE, J. C., SOLDEN, L. M., BORTON, M. A., MORIN, T. H., DALY, R. A., JOHNSTON, M. D., STEFANIK, K. C., WOLFE, R., GIL, B. & WRIGHTON, K. C. 2018. Members of the Genus Methylobacter Are Inferred To Account for the Majority of Aerobic Methane Oxidation in Oxic Soils from a Freshwater Wetland. *mBio,* 9.

SPULBER, L., ETIOPE, G., BACIU, C., MALOŞ, C. & VLAD, Ş. N. 2010. Methane emission from natural gas seeps and mud volcanoes in Transylvania (Romania). *Geofluids,* 10**,** 463-475.

STOCKER, T. F., QIN, D., PLATTNER, G.-K., TIGNOR, M., ALLEN, S. K., BOSCHUNG, J., NAUELS, A., XIA, Y., BEX, V. & MIDGLEY, P. M. 2013. Climate Change 2013: The physical science basis: Contribution of Working Group I to the Fifth Assessment Report of the Intergovernmental Panel on Climate Change. Cambridge University Press.

STOLPER, D. A., LAWSON, M., DAVIS, C. L., FERREIRA, A. A., NETO, E. V. S., ELLIS, G. S., LEWAN, M. D., MARTINI, A. M., TANG, Y. & SCHOELL, M. 2014. Formation temperatures of thermogenic and biogenic methane. *Science,* 344**,** 1500-1503.

SUZUKI, M. T., TAYLOR, L. T. & DELONG, E. F. 2000. Quantitative analysis of small-subunit rRNA genes in mixed microbial populations via 5'-nuclease assays. *Appl Environ Microbiol,* 66**,** 4605-14.

SVENNING, M. M., WARTIAINEN, I., HESTNES, A. G. & BINNERUP, S. J. 2003. Isolation of methane oxidising bacteria from soil by use of a soil substrate membrane system. *FEMS Microbiology Ecology,* 44**,** 347-354.

THOMPSON, J. D., HIGGINS, D. G. & GIBSON, T. J. 1994. CLUSTALW: improving the sensitivity of progressive multiple sequence alignment through sequence weighting, position-specific gap nealties and weight matric choice. *Nucleic Acids Research,* 22**,** 4673-4680.

TROTSENKO, Y. A. & KHMELENINA, V. N. 2005. Aerobic methanotrophic bacteria of cold ecosystems. *FEMS Microbiol Ecol,* 53**,** 15-26.

TVEIT, A., SCHWACKE, R., SVENNING, M. M. & URICH, T. 2013. Organic carbon transformations in high-Arctic peat soils: key functions and microorganisms. *ISME J,* 7**,** 299-311.

VETROVSKY, T. & BALDRIAN, P. 2013. The variability of the 16S rRNA gene in bacterial genomes and its consequences for bacterial community analyses. *PLoS One,* 8**,** e57923.

WAGNER, D., KOBABE, S., PFEIFFER, E. M. & HUBBERTEN, H. W. 2003. Microbial controls on methane fluxes from a polygonal tundra of the Lena Delta, Siberia. *Permafrost and Periglacial Processes,* 14**,** 173-185.

WALLMANN, K., RIEDEL, M., HONG, W. L., PATTON, H., HUBBARD, A., PAPE, T., HSU, C. W., SCHMIDT, C., JOHNSON, J. E., TORRES, M. E., ANDREASSEN, K., BERNDT, C. & BOHRMANN, G. 2018. Gas hydrate dissociation off Svalbard induced by isostatic rebound rather than global warming. *Nat Commun,* 9**,** 83.

WANG, Z. P., LINDAU, C. W., DELAUNE, R. D. & PATRICK, W. H. 1993. Methane emission and entrapment in flooded rice soils as affected by soil properties. *Biology and Fertility of Soils,* 16**,** 163-168.

WARTIAINEN, I., HESTNES, A. G., MCDONALD, I. R. & SVENNING, M. M. 2006. Methylobacter tundripaludum sp. nov., a methane-oxidizing bacterium from Arctic wetland soil on the Svalbard islands, Norway (78 degrees N). *Int J Syst Evol Microbiol,* 56**,** 109-13.

WEISBURG, W. G., BARNS, S. M., A., P. D. & LANE, D. J. 1991. 16S Ribosomal DNA Amplification for Phylogenetic Stucy. *Journal of Bacteriology,* 173**,** 697-703.

WHITICAR, M. J. & FABER, E. 1986. Methane Oxidation in Sediment and Water Column Environments - Isotope Evidence. *Organic Geochemistry,* 10**,** 759-768.

WHITTENBURY, R., DAVIES, S. L. & DAVEY, J. F. 1970a. Exospores and cysts formed by methane-utilizing bacteria. *J Gen Microbiol,* 61**,** 219-26.

WHITTENBURY, R., PHILLIPS, K. C. & WILKINSON, J. F. 1970b. Enrichment, Isolation and Some Properties of Methane-utilizing Bacteria. *Microbiology,* 61**,** 205-218.

WIK, M., VARNER, R. K., ANTHONY, K. W., MACINTYRE, S. & BASTVIKEN, D. 2016. Climate-sensitive northern lakes and ponds are critical components of methane release. *Nature Geoscience,* 9**,** 99-105.

WREDE, C., BRADY, S., ROCKSTROH, S., DREIER, A., KOKOSCHKA, S., HEINZELMANN, S. M., HELLER, C., REITNER, J., TAVIANI, M., DANIEL, R. & HOPPERT, M. 2012. Aerobic and anaerobic methane oxidation in terrestrial mud volcanoes in the Northern Apennines. *Sedimentary Geology,* 263-264**,** 210-219.

XIN, J. Y., ZHANG, Y. X., ZHANG, S., XIA, C. G. & LI, S. B. 2007. Methanol production from CO(2) by resting cells of the methanotrophic bacterium Methylosinus trichosporium IMV 3011. *J Basic Microbiol,* 47**,** 426-35.

YANG, S. S. & CHANG, H. L. 1998. Effect of environmental conditions on methane production and emission from paddy soil. *Agriculture Ecosystems & Environment,* 69**,** 69-80.

YOSHIKAWA, K. 1993. Notes on Open-System Pingo Ice, Adventdalen, Spitzbergen. *Permafrost and Periglacial Processes,* 4**,** 327-334.

YOSHIKAWA, K. 1998. The groundwater hydraulics of open system pingos. *Collection Nordcana,* 55**,** 1177 - 1184.

YOSHIKAWA, K. & KOICHIRO, H. 1995. Observations on Nearshore Pingo Growth, Adventdalen, Spitsbergen. *Permafrost and Periglacial Processes,* 6**,** 361-372.

YOSHIKAWA, K. & NAKAMURA, T. 1996. Pingo growth ages in he delta area, Adventdalen, Spitsbergen. *Polar Record,* 32**,** 347-352.

YUN, J., ZHUANG, G., MA, A., GUO, H., WANG, Y. & ZHANG, H. 2012. Community structure, abundance, and activity of methanotrophs in the Zoige wetland of the Tibetan Plateau. *Microb Ecol,* 63**,** 835-43.

ZHANG, J., WU, P., HAO, B. & YU, Z. 2011. Heterotrophic nitrification and aerobic denitrification by the bacterium Pseudomonas stutzeri YZN-001. *Bioresource Technology,* 102**,** 9866-9869.

Appendix

Additional results

Categorization

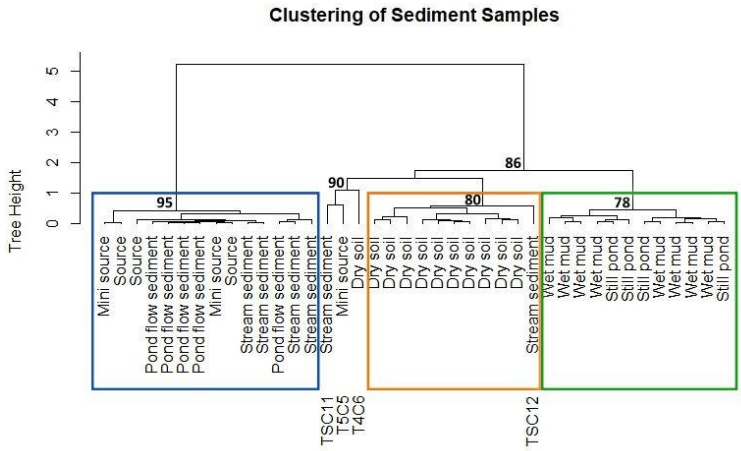

Figure 27: Clustering of sediment samples based on standardized predictor variables; three clusters are highlighted. Bootstrap values for the clusters are given above the nodes.

Figure *27*: The blue cluster combines source categories ('Mini source' and 'Source') and stream samples ('Pond flow sediment' and 'Stream sediment'). The cluster highlighted in orange contains 'Dry soil' samples and one 'Stream sediment' sample, TSC12. The cluster highlighted in green contains only 'Still pond' and 'Wet mud' samples. Not among these clusters: T4C6, T5C5 and TSC11.

Table 8: Table of relative effects of the predictor variables onto the three clusters obtained from the cluster analysis. Cluster names are derived from the colour-code in figure 28. The table can be read as in the following example: The probability that a randomly chosen sampling spot from the orange cluster has a higher pH than any randomly chosen sampling spot is 0.819, so approx. 82 %.

	Distance to the source	pH	Methane Flux	Water Content	Methane Content
Orange	0.689	0.819	0.230	0.213	0.458
Green	0.306	0.525	0.385	0.586	0.387
Blue	0.517	0.228	0.810	0.653	0.629

The non-parametric multivariate comparison test verified significant differences between the three colour-coded clusters surrogating the categories. The pH and methane fluxes have a strong influence onto the category forming, since the differences in relative effects between the clusters are large (**Table *8***). The relative effect of the water content of the 'Dry soil'-cluster is the lowest effect of all. The average water content of the 'Dry soil' sediments was 16 (± 5) %;

average water content of all other sampling spots was ~ 40 (± 7) %. Based on the significant inequality of the clusters, the decision was made to continue using the previously assigned sediment categories. This decision implies that certain observations were not given to the clustering (e.g. presence or absence of a water cover).

Pictures of the miniature sources

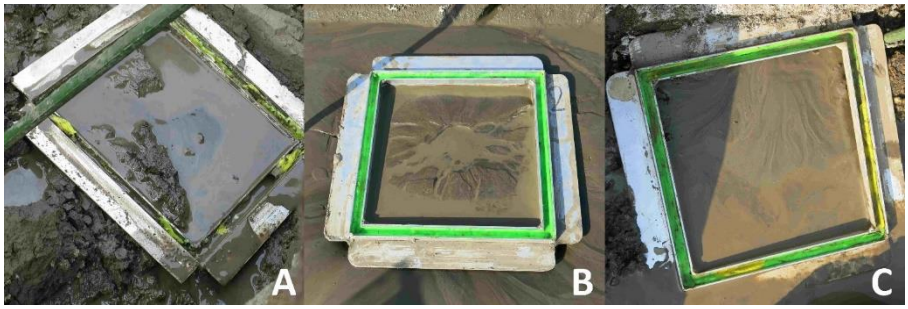

Figure 28: Pictures of the three miniature sources: **A** shows T2C4; **B** shows T4C5; **C** shows T5C5. T5C5 had a small volcano-like opening, which drowned by the accumulating water before the picture was taken. The inside of one chamber side is 20 cm long. The area inside has 400 cm^2.

Technical issues of the qPCR

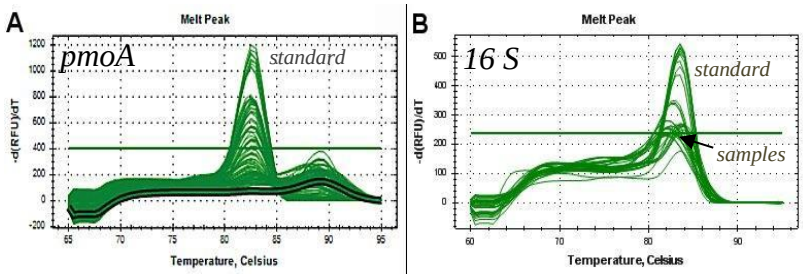

Figure 29: Exemplary qPCR output. **A**: melt peaks of *pmoA* amplification products; **B**: melt peaks of 16S amplification products. One melt peak curve from the sampling spot T5C5 is highlighted in A.

'Dry soil' samples and samples with low total DNA content frequently exhibited deviating *pmoA* products (**Figure 29**, **A**).The *pmoA* amplification of the sample T5C5 showed a peak at a different melt temperature than the standard and most samples. 'Dry soil' samples often showed two melt peaks, one at the expected temperature and one at higher temperatures. Two products were also observed with gel electrophoresis. All 16S rRNA gene amplifications exhibited singular peaks, but the melt temperature varied slightly (**Figure 29**, **B**). Moreover, low amplification efficiencies were observed for the *pmoA* qPCR. They were either 82 %, or approx. 64 %. The amplification efficiencies of the 16S rRNA amplifications were between 97.4 – 111.8 %. The R^2 values of the standard curves varied between 0.98 and 0.99, with one exception of 0.97.

Statistical criteria of the linear regression models

Table 9: Statistical criteria and parameters of the linear regression models. The last model of the table is the best-fitting model according to the stepwise forward selection, which is not shown graphically in chapter 3.1.5. pmoA = pmoA abundance, pmoAr = pmoA to 16S copy number ratio, CH4 = methane flux, CI = confidence interval, OxR = Oxidation rate, CH4c = methane content, 16S = 16S abundance.

Origin	Model	R^2	Homoscedascitiy	95% CI (intercept)	95% CI (slope)	ANOVA, F-test	*p-value* (slope)
Stream	OxR ~ pmoA	0.65	yes	± 2.24	± $0.71*10^8$	F(1, 8); F=14.687	0.005
Surface	OxR ~ pmoA	0.032	no	-	-	-	-
Stream	ln(OxR) ~ CH4	0.61	yes	± 0.31	± 0.0005	F(1, 9); F=14.111	0.0045
Surface	ln(OxR) ~ CH4	0.95	yes	-	-	-	-
Stream	OxR ~ CH4c	0.03	yes	-	-	-	-
Surface	OxR ~ CH4c	0.65	yes	-	-	-	-
Stream	pmoA ~ CH4	0.24	no (p = 0.042)	-	-	-	-
Surface	pmoA ~ CH4	0.0009	yes	-	-	-	-
Stream	16S ~ CH4c	0.04	yes	-	-	-	-
Surface	16S ~ CH4c	0.004	yes	-	-	-	-
Stream	pmoAr~CH4	0.57	no (p= 0.042)	± 3.4	± 0.12	F(1, 9); F=11.752	0.0075
Surface	pmoAr~CH4	0.25	yes	-	-	-	-
Both	OxR ~ CH4	0.59	no	± 0.67	± 0.001	F(1, 35); F=51.776	2.14×10^{-8}

Picture of T4C2

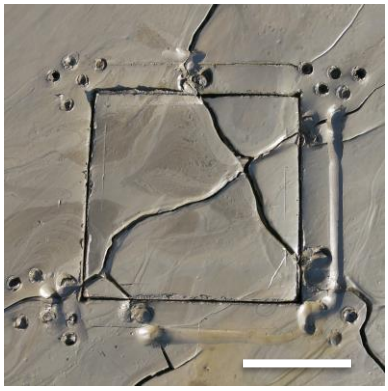

Figure 30: Picture of T4C2 as an example for cracks in the sediment layer. The white scale bar represents ~ 10 cm.

The sampling spot T4C2, from the 'Wet mud' sediment category, exhibited cracks throughout the area used for methane flux measurements. Moreover, the consistence of the sediment resembled clayey soils.

List of Protocols

Phenol-chloroform extraction total for nucleic acids as in Angel et al. (Angel et al., 2012); for modifications see 2.3.1.

Links

References

Ed Dlugokencky, NOAA/ESRL (www.esrl.noaa.gov/gmd/ccgg/trends_ch4/)

Temperature profile of Adventdalen

https://www.yr.no/nb/historikk/graf/1-2759929/Norge/Svalbard/Svalbard/Longyearbyen?q=2019 [02.05.2020, 18:15]

Sequences for the construction of the phylogenetic tree

Methylomonas trichosporium: https://www.ebi.ac.uk/ena/data/view/AAA87220 [03.03.2020, 13:15]

Methylomicrobium alcaliphilum: https://www.ebi.ac.uk/ena/data/view/CCE22213 [03.03.2020, 13:30]

Methylomonas methanica: https://www.ebi.ac.uk/ena/data/view/ACN73464 [03.03.2020, 13:40]

Methylobacter psychrophilus: https://www.ebi.ac.uk/ena/data/view/AAX48776 [04.03.2020, 09:50]

Methylobacter marinus: https://www.ebi.ac.uk/ena/data/view/ACE95886 [04.03-2020, 16:50]

Methylococcus capsulatus strain BL4: https://www.ebi.ac.uk/ena/data/view/AF533666 [04.03.2020, 16:50]

Methylosinus sporium: https://www.ebi.ac.uk/ena/data/view/ABD13902 [04.03.2020, 17:00]

Methylomicrobium pelagicum: https://www.ebi.ac.uk/ena/data/view/AAC61804 [04.03.2020, 17:05]

Methylomicrobium album BG8: https://www.ebi.ac.uk/ena/data/view/ACN73465 [04.03.2020, 17:05]

Methylomonas koyamae https://www.ebi.ac.uk/ena/data/view/QCI03775 [04.03.2020, 17:10]

Methylomonas lenta https://www.ebi.ac.uk/ena/data/view/CCW45942 [04.03.2020, 17:10]

Methylocaldum marinum https://www.ebi.ac.uk/ena/data/view/BAO51827 [04.03.202017:15]

Methylocaldum gracile https://www.ebi.ac.uk/ena/data/view/AAC04380 [04.03.2020]

Methylocaldum tepidum https://www.ebi.ac.uk/ena/data/view/AWM95755 [04.03.2020]

uncultured *Methylococcus* sp. https://www.ebi.ac.uk/ena/data/view/AVZ01024 [04.03.2020, 17:20]

Methylococcus sp. LS7-MC https://www.ebi.ac.uk/ena/data/view/ALO24369 [04.03.2020]

Methylosarcina lacus https://www.ebi.ac.uk/ena/data/view/AAG13081 [11.03.2020, 14:00]

Buffer and Media Compositions and Reagents

for nucleic acid extraction

TNS - extraction buffer modified from (Henckel et al., 1999)

500 nM TRIZMA (M.W. 121.14 g/mol; 15.76 g), 100 mM NaCl (M.W. 58.44 g/mol; 1.17 g), 10% SDS (M.W. 288.38 g/mol; 20g), 200 mL RNase-free water, dissolve and autoclave

PEG-6000

37.4g NaCL & 120 g of polyethylene glycol in 400 mL DEPC-treater water

Phenol Chloroform Isoamylalcohol

ratio = 25:24:1; pH 6.6-7.9

Chloroform Isoamylalcohol

ratio = 24:1

for enrichment and isolation

NMS – Nitrate Minimal Media – DSMZ medium 921

Used at a 0.1 x dilution. For buffer composition follow:

https://www.dsmz.de/microorganisms/medium/pdf/DSMZ_Medium921.pdf

TGGA agar plates

5 g Tryptone, 2.5 g Yeast extract, 1 g Glucose, 20 g Agar, fill up to 1 L with water, mix, autoclave

for FISH

PBS – Phosphate buffered saline

0.4 M NaCl (Merck, Darmstadt, Germany), 0.03 M $NaPO_4$

Storage Solution

0.1 % Tergitol NP_{40} (Sigma-Aldrich) with 4% (v/v) 1M (VWR, Radnor, USA) pH 7.5

Hybridization solution (20% formamide)

0.9 M NaCl, 0.1 M Tris pH 7.5, 20% (w/v) Formamide (VWR, Radnor, USA), 10% (w/v) SDS (Merck, Darmstadt, Germany)

Washing solution 1

0.9 M NaCl, 20 mM Tris pH 7.5, 0.01% (w/v) SDS

Washing solution 2

0.18 M NaCl, 20 mM Tris pH 7.5, 0.01% (w/v) SD

Primer & probe sequences

	Type	Sequence (5' to 3')	Publication
BAC1369F	primer	CGGTGAATACGTTCYCGG	(Suzuki et al., 2000)
BAC1492R	primer	GGTTACCTTGTTACGACTT	(Weisburg et al., 1991)
A189F	primer	GGN GAC YGG GAT TTC TGG	(Holmes et al., 1995)
Mb601R	primer	ACRTAGTGGTAACCTTGYAA	(Kolb et al., 2003)
Mb661R	primer	CCGGMGCAACGTCYTTACC	(Costello and Lidstrom, 1999)
Mg64	probe	CCGAAGGCCTRTTACCGTTC	(Bourne et al., 2000)
EU338	probe	GCTGCCTCCCGTAGGAGT	(Amann et al., 1990)

Additional information

Weight to volume conversion factor

$$Weight\ to\ volume\ conversion\ factor = \frac{V_{s.b.}[mL] - V_{r.s.}[mL] - V_{headspace}[mL]}{m_{sample}\ [g]} \quad \mathbf{4}$$

With V being the volume, m being the mass; "s.b." shortens the index "serum bottle" and "r.s." shortens the rubber stopper. Only the part of the rubber stopper that is inside the serum bottle is regarded for this equation.